UNIVERSIDADE DA BEIRA INTERIOR
Engenharia

3D CFD Simulation of a Cold Flow Four-Stroke Opposed Piston Engine

Robert Silva Gonçalves

Dissertação para a obtenção do Grau de Mestre em
Engenharia Aeronáutica
(Ciclo de estudos integrado)

Orientador: Prof. Doutor Francisco Miguel Ribeiro Proença Brójo

Covilhã, Outubro de 2014

Dedication

To my parents, for the effort, sacrifices and hard work carried through over these years.

To my fantastic sister for being my constant companion.

For my dedicated grandmother and for my grandfather who did not have the opportunity to witness this important moment of my academic career.

"Simplicity is the ultimate sophistication"

Leonardo da Vinci

Acknowledgments

I would like to thank, above all, my parents and my sister. Their love and support were crucial for my academic success. I love you very much!

I thank my supervisor, Professor Francisco Miguel Ribeiro Proença Brójo, whom I respect greatly, for all the knowledge, patience, support and time spent during this process. I will forever remember everything you have done for me.

I would also like to acknowledge the ANSYS Support team, with special attention to Mr. Jorge Izquierdo and Mr. Pedro Afonso for their availability. Their help was of great importance.

I wish to thank my soul mate, Sandra Gonçalves, for being so patient, kind and supportive. I love you!

I want to thank all my friends, scattered around the country and the world for being my second family.

Thank you, Cecilia Albuquerque for aiding and encouraging me during these years.

Resumo

É realizada uma simulação em CFD de um motor de pistão oposto a funcionar num ciclo de quatro tempos. Pretende-se avaliar o comportamento e as propriedades do escoamento dentro do cilindro, de forma a viabilizar o seu uso a nível comercial. Devido às características inerentes de um motor de pistão oposto, torna-se assim necessário dimensionar o modelo, tendo como referência o motor Jumo 205E: ambas as válvulas, bem como a câmara de combustão e as portas de escape e admissão. Uma câmara de combustão adjacente à zona do cilindro é criada de modo a poder colocar as válvulas. O software comercial *Fluent 14.0* é escolhido para realizar os cálculos numéricos. Dada a complexidade do estudo, maioritariamente devido às partes móveis existentes, o uso da malha dinâmica é necessária. O modelo *Standard* $\kappa - \varepsilon$ é o escolhido para o modelo da viscosidade; as portas de entrada e saída de ar são definidas como *pressure-inlet* e *pressure-outlet*, respetivamente. PISO e PRESTO! são os métodos de cálculo usados para o acoplamento pressão-velocidade e discretização pressão, respetivamente. Os resultados obtidos não foram os esperados, dado o comportamento e propriedades inadequados do fluido no cilindro e portas.

Palavras-chave

Admissão; Escape; CFD; *Fluent*; Pistão oposto; Motor de combustão interna

Resumo Alargado

É realizada uma simulação em CFD de um motor de pistão oposto a funcionar num ciclo de quatro tempos . Pretende-se avaliar o comportamento e as propriedades do escoamento dentro do cilindro, de forma a viabilizar o seu uso a nível comercial. Tendo em conta o historial deste motor, é de um grande interesse realizar uma adaptação do mesmo; inúmeros parâmetros obtiveram o seu nível *standard* devido às caracterícas do motor de pistão oposto. Um motor deste tipo, não tendo cabeça de cilindro, dificulta a tarefa de colocar as válvulas de um modo que o seu funcionamento seja eficiente. É assim necessário dimensionar o modelo, com base no motor de referência Jumo 205E: ambas as válvulas, bem como a câmara de combustão e as portas de escape e admissão.

A construção do modelo, bem como a decomposição, geração da malha e o cálculo da solução são feitos a partir de software comerciais: o *CATIA V5* e o *ANSYS* (o software *ANSYS* possui várias funcionalidades que permitem realizar as tarefas exigidas). Com a construção do modelo concluída, este é decomposto no *ANSYS Design Modeler* onde diversas zonas são definidas (oito no total), entre elas o *inboard* e o *vlayer*. Estes objetos são colocados junto à superfície superior das válvulas de modo a evitar deformações agressivas na malha. Nomeiam-se as superfícies e zonas para melhor entendimento do modelo. No *ANSYS Meshing* a malha é criada com um total de 3638149 elementos, onde ambas, malha estruturada e não estruturada, são usadas: a primeira é utilizada nas zonas com formas cilíndricas tais como o cilindro, *inboard* e o *vlayer*; a segunda é usada nas zonas com uma geometria mais complexa como a câmara de combustão e ambas as portas. Por fim, a modelação da solução é realizada ao recorrer do software comercial *Fluent 14.0*. *Standard* $\kappa - \varepsilon$ é o modelo escolhido para a viscosidade, bem como o modelo de energia é ativado. No que toca às condições de fronteira, a entrada de ar é definida como *pressure-inlet* e a saída de ar como *pressure-outlet*. O uso da malha dinâmica é necessário devido ao movimento dos pistões e das valvulás: todos os três métodos são ativados (*layerng*, *remeshing* e *smoothing*). A solução usada para o acomplamento da pressão-velocidade é o PISO e para a discretização da pressão o PRESTO!. São definidos um total de 2440 passos e um valor máximo de 40 iterações por passo, que equivale a 600º.

O resultado obtido não foi o desejado. O comportamento do fluido tanto no cilindro, como nas portas, era inadequado para o bom funcionamento de um motor. A possibilidade de ainda obter bons resultados neste aspecto é credível dada às inúmeras variáveis existentes neste ramo. O uso de motores com volumes mais pequenos será certamente um início para trabalhos futuros.

Abstract

A CFD simulation of a four-stroke opposed piston engine has been performed. It is intended to evaluate the overall behavior and properties of in-cylinder flow, in a way that its use comercialy can be achieved. Due to the inherent characteristics of an opposed piston engine, it is necessary to dimension the model, using as reference the Jumo 205E engine: both valves, as well as the combustion chamber and both exhaust and admission ports. A combustion chamber adjacent to the cylinder zone is placed in order to fit both valves. The commercial software *Fluent 14.0* is used to perform the numerical calculations. Due to the complexity of this study, mostly because of the existence of moving parts, the use o dynamic meshing is necessary. The viscous model is *Standard* $\kappa - \varepsilon$; the port entry and exit are defined as *pressure-inlet* and *pressure-outlet*, respectively. PISO and PRESTO! are the chosen methods for pressure-velocity coupling and pressure space discretization, respectively. The final results obtained were far from the expected, mainly due to the inadequate behavior and properties of the fluid within the cylinder and ports.

Keywords

Admission; Exhaust; CFD; *Fluent*; Opposed piston; Internal combustion engine

Contents

List of Figures

List of Tables

List of Acronyms

AMG	Algebraic Multigrid Method
ARS	Algebraic Reynolds Stress
BDC	Bottom Dead Center
BMEP	Break Mean Effective Pressure
BTE	Break Thermal Efficiency
CFD	Computational Fluid Dynamics
CI	Compression Ignition
CO	Carbon Monoxide
CPU	Central Processing Unit
DNS	Direct Numerical Simulation
EVM	Eddy Viscous Models
HC	Hydrocarbons
HWA	Hot Wire Anemometer
IC	Internal Combustion
IDC	Inner Dead Center
IGES	Initial Graphics Exchange Specification
IMEP	Indicated Mean Effective Pressure
LDV	Laser Doppler Velocimetry
LES	Large Eddy Simulation
LPG	Liquefied Petroleum Gas
NRC	Nuclear Regulatory Commission
OP	Opposed Piston
OPOC	Opposed Piston Opposed Cylinder
PISO	Pressure-Implicit with Splitting of Operators
PIV	Particle Image Velocimetry
PRESTO!	PREssure STaggering Option
R&D	Research and Development
RAM	Random Access Memory
RANS	Reynolds-Averaged Navier-Stokes
RNG	Re-Normalization Group
RSM	Reynolds Stress Models
SA	Spalart-Allmars
SFC	Specific Fuel Consumption
SI	Spark Ignition
TDC	Top Dead Center
UAV	Unmanned Aerial Vehicle
UK	United Kingdom
URF	Under-Relaxation Factors

Nomenclature

a	Crank offset	$[m]$
A_{act}	Actual area	$[m^2]$
A_{cur}	Curtain area	$[m^2]$
A_{min-ex}	Minimum exhaust valve area	$[m^2]$
A_{min-in}	Minimum exhaust valve area	$[m^2]$
A_P	Piston face area	$[m^2]$
A_R	Reference area	$[m^2]$
AF	Air-fuel ratio	$[-]$
AF_{act}	Actual air-fuel ratio	$[-]$
AF_{sto}	Stoichiometric air-fuel ratio	$[-]$
B	Bore	$[m]$
$BMEP$	Break mean effective pressure	$[Pa]$
c	Speed of sound	$[m/s]$
c_{ex}	Speed of sound at the exhaust valve	$[m/s]$
c_{in}	Speed of sound at the intake valve	$[m/s]$
c_r	Compression ratio	$[-]$
C	Courant number	$[-]$
	Constant of value 1.3	$[-]$
C_D	Discharge Coefficient	$[-]$
D	Diameter	$[m]$
D_v	Valve Diameter	$[m]$
e	Total energy	$[J]$
f	Body force per unit mass	$[N/kg]$
FA	Fuel-air ratio	$[-]$
FA_{act}	Actual Fuel-air ratio	$[-]$
FA_{sto}	Stoichiometric Fuel-air ratio	$[-]$
g_x, g_y, g_z	Acceleration (x, y and z, respectively)	$[m/s^2]$
$IMEP$	Indicative mean effective pressure	$[Pa]$
k	Thermal conductivity	$[W/m \cdot K]$
l	Piston position	$[m]$
L	Stroke	$[m]$
L_{ex}	Exhaust valve lift	$[m]$
L_{in}	Intake valve lift	$[m]$
L_v	Valve lift	$[m]$
$\dot{m}$	Mass flow	$[kg/s]$
m_a	Mass of air	$[kg]$
$\dot{m}_a$	Mass flow of air	$[kg/s]$
m_f	Mass of fuel	$[kg]$
$\dot{m}_f$	Mass flow of air	$[kg/s]$
M	Mach number	$[-]$
n	Number of revolutions	$[-]$
N	Engine speed	$[rpm]$
N_c	Number of cylinders	$[-]$
p	Pressure	$[Pa]$

p_0	Downstream pressure	$[Pa]$
p_{atm}	Atmospheric pressure	$[Pa]$
p_T	Upstream Pressure	$[Pa]$
P	Power	$[W]$
Pr	Prandtl number	$[-]$
$\dot{q}$	Heat flux	$[W/m^2]$
r	Connecting rod length	$[m]$
R	Connecting rod length-to-crank offset ratio	$[-]$
	Ideal gas constant	$[J/K \cdot mol]$
Re	Reynolds number	$[-]$
RS	Reference Size	$[m]$
SFC	Specific fuel consumption	$[kg/W \cdot s]$
t	Time	$[s]$
T	Temperature	$[K]$
T_0	Downstream temperature	$[K]$
u, v, w	Velocity components according to x, y and z	$[m/s]$
U	Velocity	$[m/s]$
U_P	Piston velocity	$[m/s]$
$U_{P_{max}}$	Maximum piston velocity	$[m/s]$
V_{BDC}	Volume at bottom dead center	$[m^3]$
V_c	Clearance volume	$[m^3]$
V_d	Displacement volume	$[m^3]$
$\dot{W}$	Work rate	$[W]$
W_b	Break work	$[J]$
W_i	Indicative work	$[J]$
x	Cell length	$[m]$
X_{ex}	Vector of exhaust valve angles	$[-]$
X_{in}	Vector of intake valve angles	$[-]$
x, y, z	Coordinate system	$[-]$
Z	Index Mach number	$[-]$

Greek letters

α	Thermal diffusivity	$[m^2/s]$
	Valve area ratio	$[-]$
β	Bore-to-stroke ratio	$[-]$
	Diffusion number	$[-]$
ϕ	Equivalence ratio	$[-]$
γ	Heat capacity ratio	$[-]$
η_m	Mechanical efficiency	$[-]$
η_V	Volumetric efficiency	$[-]$
μ	Dynamic viscosity	$[Pa \cdot s]$
ν	Kinematic viscosity	$[m^2/s]$
π	Constant of value 3.14159…	$[-]$
θ	Crank angle	$[°]$
θ_{IVC}	Crank angle at closed intake valve	$[°]$
θ_{IVO}	Crank angle at opened intake valve	$[°]$
ρ	Density	$[kg/m^3]$

σ	Normal stress	[Pa]
τ	Torque	[$N \cdot m$]
	Shear stress	[Pa]

Chapter 1

Introduction

1.1 Motivation

The Opposed Piston (OP) engine was initially designed in the late 1800's in Germany as an alternative to the existing engines of the time, such as the Otto engine, and was well known for its versatility and simplicity in numerous applications which included aircraft, ships, tanks, locomotives, automobiles and stationary [1]. Even though the OP concept could be applied to both two and four-stoke diesel engines, the two-stroke cycle was predominant, probably for simplicity reasons, while the most noticeable four-stroke OP engine was built by a French manufacturer, Gobron Brillié, and was used as a racing engine, around 1900.

The advantages presented by the two-stroke OP engine were so great, that several records, which were established at the time, are yet to be equaled. These records have set the regular standards which are still used today for power-to-weight ratio, dynamic refinement, fuel tolerance, package space, fuel efficiency and manufacturing simplicity. The advantages involved many important aspects which significantly improved the performance of the engine overall; ease of manufacture, excellent balance, fuel efficiency, outstanding specific output, high specific torque, very high power density and power-to-bulk ratio. Also, two-stroke cycles presented greater benefits compared to the conventional four-stroke engine: heat transfer reduction with fewer loss in engine friction and mechanical durability, reduction of the number of cylinders, therefore reducing the surface area, effective stroke-to-bore ratio could be done without compromising piston speed, very reliable, low maintenance, excellent multi-fuel tolerance, low injection pressures along with simple fuel injection nozzles and a very low part count.

With the implementation of emission regulations in the mid-20th century, the rise of the OP engine came to a halt, mainly due to oil consumption and high emission problems, allowing the conventional four-stroke engine to develop further. Among the typical challenges which two-stroke engines faced, the main issues involved lubrication of the small-end bushes and piston-pin bosses, port traversing by the rings, side injection and torsion vibration. In four-stroke OP cycle engines, the most difficult challenge, in addition to the problems presented by the two-stroke cycle engine, was still the location of the admission and exhaust valves, which will be one of the topics covered in this study.

The OP engine is still used in many unconstrained emission level applications; however, with the increasingly tighter emission regulations, the technology available today, along with the different manufacture processes and larger number of solution possibilities, many of the problems regarding the OP engine could be overcome and a wider field of application may appear. Therefore, it is of great interest to focus on this subject in order to develop and improve Internal Combustion (IC) engines, and perhaps re-launch the OP engine.

The aeronautical sector could benefit greatly from the success of four-stroke OP engines, mainly

due to its power-to-weight ratio, a very important factor in aeronautic projects. Even though only lighter aircraft would benefit more from the OP engine, the applications are numerous. Unmanned Aerial Vehicles (UAV) are a perfect example of a low-risk possibility to apply the OP engine, for both fixed- and rotating-wing aircraft, powered gliders and ultralight aircraft. Despite being a good alternative for future UAV's, the widely used two-stroke Boxer engine still remains a strong competitor in the 8 kW range field. In 80 kW UAV's statistical analysis by comparing the OP engine with the Wankel engine shows a slight advantage of the OP in several aspects, such as fuel efficiency and estimated cost. In addition, the size of the OP engine is 20% smaller than the Wankel and possesses a bulk four times greater.

Despite the importance of the IC engine to society, it has a great impact on the environment and on public health, which worsens with the increase of the already vast number of motored vehicles. A rapid solution is therefore necessary, not only for these reasons but also due to the limited fuel reserves. During the last century, the IC engine efficiency has been improved greatly, however it is well documented that it is still inefficient and therefore, possible solutions are being developed, yet unsuccessfully. The Nuclear Regulatory Commission (NRC), concluded that the IC engine will most likely be the prime mover for the next years, possibly decades. Thus, it is important to continue Research and Development (R&D) in this area, in order to better understand its fundamental processes affecting engine efficiency and the production of undesirable emissions [2].

1.2 Main Goals

Engineering tasks, such as structural and fluid analysis, have become simpler due to the appearance of computational software, improving the way of how engineers face obstacles: it is more economical, the analysis can be done faster, results are less prone to errors and, if necessary, adjustments can be performed quickly.

The present work focuses on the construction of a four-stroke OP engine model, based on the Jumo 205E engine, followed by a numerical analysis using Computational Fluid Dynamics (CFD) tools, with the purpose of verifying its reliability of the selected valve positioning and engine geometry. Also, port flow behavior is studied in order to understand the influence of the port design during admission and exhaust processes.

1.3 Task Overview

In the present chapter, the author expresses his motivation behind the development of this thesis, presenting what is intended to be achieved and the reasons which led to it. The objectives for this study are also outlined and presented in a brief review regarding the OP engine as well as its operating mode. Finally, a bibliographic review is presented, focusing on other works related to the subject and pointing out their importance in this area.

In chapter 2, the basics of the IC engine analysis are discussed, such as the basic operating parameters. The effects of turbulence on different aspects during each cycle and the behavior of the gas during the exhaust and intake processes are also discussed.

Chapter 3 provides a deeper insight into the government equations of CFD analysis; the appropriate turbulence models are also discussed. The construction of the geometry in study is explained, as well as the generation of the mesh and dynamic mesh used for the simulation. Boundary conditions are imposed and the solution method is chosen.

Chapter 4 presents the numerical results obtained by the CFD simulation. The results are explained in detail and discussed throughout this chapter. Possible problems encountered in this thesis are mentioned as well.

Chapter 5 presents the conclusions from the simulation in CFD and provides suggestions for future work.

1.4 Historical Review

In the mid-19th century, the development of the IC engine was based on single-cylinder engines and both two- and four-stroke engines, which offered simplicity and higher efficiency. The OP concept initially offered an attractive way of achieving a very dynamic and balanced single-cylinder engine that eliminated the need for cylinder-head joints and avoided the challenges in manufacturing a monolithic cylinder with cylinder-head barrel. The "double" stroke presented another significant advantage – the possibility of large-cylinder displacements with small-cylinder bores, reducing gas loads on the crankshafts. The development of the OP engine can be divided into three main periods: pre-1900, from 1900 until the end of World War II in 1945 and from then on.

1874 - 1900

In 1874, Giles of Cologne built an OP, single-cylinder engine with one of the pistons connected to the crankshaft, while the other was a free piston. The crank-driven piston would induce a fresh charge from a cam-actuated inlet port, located approximately mid-cylinder. The charge would then ignite partway through the expansion of the crank-driven piston, causing a rise in pressure and the retraction of this piston, while the free piston would be displaced until its end stop, being then retained by a controlled clutch in order to drive out the exhaust products. Although a large amount of these engines were produced, they were never commercially successful, especially due to the thriving Otto four-stroke engine.

The production of the first OP engine with both pistons being crank-driven is ascribed to Wittig. Even though this has not been proved [3], Wittig did introduce the classical three-throw crank, where the center throw is linked to the inner-piston (closest to the crankshaft) and both outboard throws, phased at 180º relatively to the center throw, are linked via rods to the outer-piston (furthest from the crankshaft), as shown in Fig. 1.1. Admission and exhaust were done by ports located in the middle of the cylinder and operated on a four-stroke basis. The most significant advantage of this concept was the cancellation of forces acting on the main bearings, as a two-piston system respects Newton's 3rd Law of Motion, producing essentially equal and opposite net gas and inertia forces.

T.H. Lucas later introduced the two crankshaft OP engine, where the upper driving crankshaft

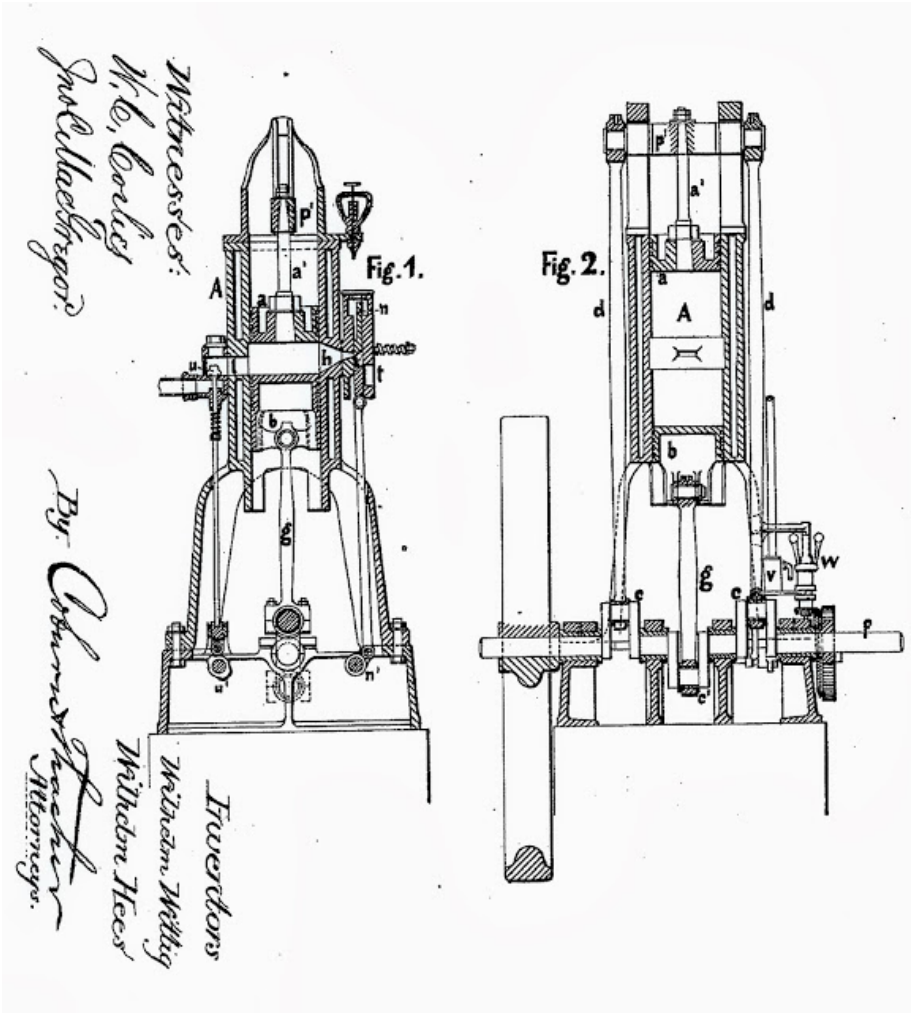

Figure 1.1: Schematics of the Wittig Gas Engine, 1879 [4]

had a large flywheel (a large wheel, mounted on the crankshaft whose function is to maintain its speed constant, by storing the excess energy from the power stroke, being later returned during the next stroke [5]) and the lower crankshaft had several gearing arrangements enabling it to move in a prescribed manner relative to the upper crankshaft. Being a two-stroke engine, it became unique due to the non-existence of scavenging (in the traditional four-stoke sense) and induction was achieved by positive displacement of both pistons.

In 1892, Robson of Sunderland presented a variant of the Wittig engine, in which the cranks were arranged differently in order to avoid both pistons reaching their dead centers simultaneously. This concept was very close in principle to the famous Oechelhaeuser and Doxford that would be developed, also in Sunderland, 20 years later.

The most notable breakthrough in the subject before 1900 was definitely the two-stroke OP gas engine developed by Hugo Junkers and Oechelhaeuser in 1892, at the Gas Engine Research Institute. The output of the 3 l engine was 84.3 kW at 160 rpm, with a mechanical efficiency of 77%. This was, and still is, an astonishing achievement, while simultaneously fuel consumption was reduced by 40% when compared to the contemporary four-stroke engine. By the end of the century, the advantages of the concept became obvious: simplicity, light mechanical loading of the crankshaft, balance and the no need for a cylinder head joint.

1900 - 1945

The development and research of the OP engine before 1900 was a success, and the years from the beginning of the 20th century until the end of World War II also witnessed several achievements, initially marine and stationary, and later on in aviation. Many people participated in these achievements. Among them was R. Lucas with the introduction of many conceptual aspects and the notable importance given to the crankcase compression pressure, which minimized the crankcase volume.

Beardmore & Oechelhaeuser also played an important role in the development of OP engines with numerous features, such as the location of the oil scraper rings on the cylinder bore, consequently reducing the overall height of the engine. Further variants enabled overall height reduction (35% lower than the traditional Oechelhaeuser engine), reduced pump losses, inertia loads, higher speeds and mass of moving parts even though these engines would often suffer connecting rod fractures.

Fullagar developed the gas engine and improved OP packaging and weight reduction. Despite the reliability of these engines, their performance at certain speeds was not the desired one and regardless of all rectifications, this project was dismantled along with several others. The Fullagar concept was later applied to the 115 Q and R engines, remaining in service for 15 years with no severe faults, with high Break Thermal Efficiency (BTE) and being highly acknowledged for their simplicity, robustness, efficiency and longevity.

Hugo Junkers, already referenced, developed the tandem engine and was involved in various engine applications. In the field of aeronautics, special attention was given to the Fo2, and later to the Mo3. Both, despite their success, were destroyed as a result of the conditions imposed by the Treaty of Versailles in 1918. Afterwards, Junkers manufactured the Fo4, a derivation of the Fo2, and after a series of developments, Jumo 4 appeared, being later renamed as Jumo 204. Until the beginning of World War II, Junkers suffered an evolutionary period, focusing mainly on aero engines and, amongst several models, the Jumo 205 (Fig. 1.2) and 207 entered production, with the 205 becoming the first engine for commercial applications and the 207 being used in high-altitude applications.

Doxford's OP engines had a big impact on the marine sector, but eventually proved to be inapt for the industry. D. Napier had a significant impact on the engine business, especially with the Napier Lion, which powered World War I aircraft and naval powerboats (W12 Napier Lion), and he established a world record in speed set by the Gloster VI Seaplane with a top speed of 565.36 km/h, in 1929. Other engines were later manufactured and widely used in World War II, such as in the Mustang and Typhoon fighter aircraft. Finally, the Sulzer brothers took an attempt on OP engines; however, they were unsuccessful due to the large engine height required to operate at very low marine speeds.

1945 - Today

After World War II, the OP engine unexpectedly experienced the most fruitful manufacturing period, especially with United Kingdom (UK) companies, despite the fact that its use reduced dramatically. This period brought the equilateral triangle arrangement - a Napier Deltic design,

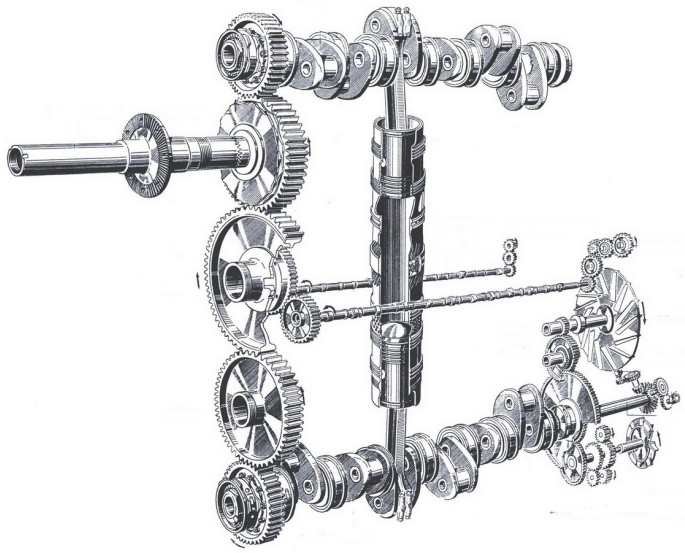

Figure 1.2: Schematics of the Junkers Jumo 205E [6]

the K60 and K60T from Rolls Royce Motors and more recently, the Diesel Air Engine – Air Airship Industries. Among these, the Opposed Piston Opposed Cylinder (OPOC) has received very positive feedback from most industries. Reference [3] provides an excellent insight into OP engines regarding this period for those who desire to extend their knowledge in this subject.

1.4.1 Operating Conditions

Normally, OP engines are characterized by a pair of pistons operating in a single cylinder, eliminating the need of cylinder heads, with slight variations in the disposition of the engines' components. There are several types of OP engines, essentially five, with many variants which will be briefly described.

The Crankless OP Engine

The crankless OP engine, also known as the free piston engine, commonly displays its pistons in a single-cylinder with the necessary space between them for combustion. Both pistons are connected to a pneumatic spring or a bounce chamber, allowing them to return to their Inner Dead Center (IDC), after combustion and expansion. The engine starts with the help of compressed air and the bounce pistons need air replenishment in order to maintain the minimum pressure levels required. There is no more further information about this variation of engine.

The Single-Crank OP Engine

The next type of OP engine is the Single-Crank OP engine, which has two main variations: the three-throw crankshaft (Wittig) and the folded rockers. As mentioned in the previous section (Sec. 1.4), the first OP engines produced in 1878 used the first type of arrangement mentioned above: a single three-throw crankshaft in which three connecting rods, each phased at 180º from each other, connected to both pistons. The central rod drove the "inner" piston (which

was closer to the crankshaft), while the remaining side rods drove the "outer" piston (which was farther from the crankshaft).The rotating movement of the crankshaft moved both pistons in order to produce the equivalent linear movement seen in normal piston engines. Numerous benefits were obtained from this arrangement, namely the fact that the moving parts and the cylinder liner contained all of the gas and inertia loads, which resulted in practically no transmission of these loads, other than the torque reaction forces to the engine frame or the main bearing. This advantage allowed the engine to be relatively lightweight due to the light crankcase. The downside of this arrangement led to a longer crank, when compared to other equivalent-displacement single-cylinder OP engine arrangements.

The folded rockers OP engines had a completely different design when compared to the previous variation. The pistons were connected to a single crankshaft by combining several rocking beams, which were essentially pivoted levers with an articulated joint. In this case, the rockers were subject to large bending loads, thus the rocker shafts that supported the rockers needed to withstand the extensive loads by using strong tensile elements, such as crossbolts. Similarly to the single-crank OP engine, all loads were carried by the cranktrain and the crossbolts, resulting in a relatively light crankcase once again. This, along with the folded arrangement, allowed the overall size of the engine to be reduced significantly, in some cases about 50%.

The Double Crankshaft OP Engine

The double-crankshaft OP engine, introduced by T.H. Lucas (Sec. 1.4), brought an advantage in relation to the single-crankshaft OP engine by presenting more compact inline arrangements. Both crankshafts were connected by spur gears, bevel gears and lay-shafts, or chain drives. By comparing basic height and length of the twin-crankshaft arrangement with the single-crankshaft layout, the latter presented a height 15% lower than the twin-crankshaft, but had an increase of length by 250% for the same displacement. The ratio of their bore dimensions was taken into account in this comparison. Depending on the application desired, the single-crankshaft layout tended to be less favorable than the twin-crankshaft arrangement, mostly due to adverse torsion vibration characteristics. However, a new concept of the single-crankshaft has been studied, the OPOC, which reduces the above mentioned length disadvantage. A multiple-crankshaft OP engine is another variant which is essentially a combination of multiple twin-crankshafts in various geometric forms (triangle, square or star).

The Rotary OP Engine

A more improbable variation is the rotary OP engine, where the pistons are somewhat like paddle blades and oscillate about a central output shaft, while the whole assembly is contained in a cylindrical housing that holds the combustion and gas-exchange systems. In some cases, the pistons orbit as well as oscillate and can perform either two-or-four-stroke cycles with appropriate ports.

The Barrel OP Engine

Finally, the barrel cam engines function in a way that the cylinders are parallel to the crankshaft axis and the pistons engage with a cylindrical cam track, which forms part of the crankshaft.

Aeronautical OP Engines

During the 20th century, several aeronautical OP piston engines emerged; however, only two variations had an important impact on this area: the Junkers Jumo 205 and the current Diesel Air Engine. The Jumo 205, also used in military applications, is still considered the most efficient aero piston engine in aviation, as it was the only diesel engine used regularly in aircraft service and was produced in large quantities. It is based on a vertical liquid-cooled light-alloy cylinder arrangement with two crankshafts driving the upper exhaust pistons and the lower air pistons. The air crankshaft drives a geared centrifugal blower which supplies scavenge air and the exhaust crankshaft drives the airscrew; fuel injection pumps for each cylinder are activated by two camshafts located at the center of a set of five spur gears which are connected to both crankshafts. The coolant pump, lubrication oil pressure and scavenge are controlled by a single shaft at the rear of the air crankshaft with each of the low-oil pressure fuel pump systems being driven off the rear end of each camshaft. The two inlet manifolds are integrally casted with the cylinder block and its entries are located on the rear face of the crankcase and connected with the twin outlets of the centrifugal blower. The liner is considered the best component of all components of the engine in terms of design, materials, finish and its contribution for engine performance and durability.

1.5 Bibliographic Review

For decades, understanding in-cylinder flow has been a great challenge for engineers due to the great number of events taking place in a very short period of time. In order to analyze and study these events, several techniques are often used, such as Hot Wire Anemometer (HWA), Laser Doppler Velocimetry (LDV) and Particle Image Velocimetry (PIV). These techniques, however, have their limitations and are very expensive - better results are proportional to greater costs. An excellent review of these methods is done by [7], where both advantages and limitations are explained in detail. With the emergence of new tools, such as CFD, IC engine analysis took a step forward. It is important to know that despite all its advantages, the user must be aware that CFD results are only predictions and can be, at times, far from accurate [8]. Both experimental data and numerical simulations should be used together in order to make better decisions regarding the outcome of the project. Nevertheless, when used correctly, CFD can be a very important and helpful tool, which can be noticed in the increasing number of studies performed in turbo machinery with its use.

The number of numerical simulations studies of IC engines is very vast and have numerous approaches. Unfortunately, no study involving four-stroke OP engines has been found and, thus, this section will mainly focus on the numerical aspect of the studies and their results in order to have a baseline to know what to expect from the OP engine.

Regarding OP engines, in 2010, [9] performed a three-dimensional computational study of scavenging performance in a two-stroke OP engine. Two models were studied: the first with two admission ports and one exhaust port; the second model had four admission ports and one exhaust port. Both models were built symmetrically in order to reduce the number of cells which were 29298 and 112667 cells, respectively. *Fluent* was the software of choice to perform the simulation. *Standard* $\kappa - \varepsilon$ was selected for the viscous model, PRESTO! and PISO for the pres-

sure discretization and pressure-velocity coupling, respectively. As for the boundary conditions, the intake was defined as *pressure-inlet* whereas the exhaust as *pressure-outlet*.

The authors concluded that, for both cases, the best intake pressure for optimum scavenging was 1.1 atm and for the same admission pressure the second model presented better scavenging efficiency, delivery ratio and trapping efficiency.

Still regarding OP engines, [10] performed a computational study as well in this field, in 2012. A single cylinder, two-stroke OP engine simulation was done in order to understand scavenging performance at different scavenging pressures and engine performance at full load. The supercharged engine model possessed two ports: one admission and one exhaust opposed to each other. Boundary conditions are calculated by *Matlab*, whilst the gas flow is computed by the one-dimensional commercial code *GT-Power*. A cylinder with one piston is modeled, with the same bore as of the OP engine model, as well as an equivalent single piston motion profile to assure that the expanding work stayed invariant. Heat and combustion processes are also included in the study.

The analysis showed that engine speed in OP engines has a strong influence in volumetric efficiency and mass flow rate, as well as the occurrence of backflow. Volumetric efficiency increased with engine speed, however started to decrease when engine speed reached 2000 rpm. Also, the greater the engine speed value, more likely it is to occur backflow. Both pressure and temperature profiles showed to be very similar to conventional engines.

With respect to numerical studies of OP engines, the review has been concluded. The following reviews are related to other aspects of in-cylinder analysis.

On the subject of CFD modeling of in-cylinder analysis, [11] presented a study on general *Fluent* modeling of an IC engine. In this paper the author studied the tutorial model offered by *ANSYS* in order to predict in-flow movement, with no combustion, by using the *In-Cylinder* model of the referred software. Using the *ANSYS Workbench* capabilities, the geometry was decomposed into 6 fluid zones, each one with their own mesh type and size. Cells were placed in a region considered as the minimum valve lift in order for the solution to function properly. Also, events were created at defined moments of piston motion. Likewise the first review, *pressure-inlet* and *pressure-outlet* were chosen for intake and exhaust boundary conditions, respectively. *Standard* $\kappa - \varepsilon$ was chosen for the viscous model and PISO was used as the pressure-velocity coupling scheme. The time-step was set to 0.25° for this case and decreased during valve openings to 0.125°. Finally, initial engine temperature was defined as 300 K since it was considered that the engine was naturally aspirated.

It was concluded that the software can perform effectively all four-strokes of the IC engine, giving good detail on air mixing and turbulence, as well as accurate temperature and pressure profiles.

[12] used *Fluent* as well, in order to study the performance of a three-dimensional two-stroke Spark Ignition (SI) engine. Based on experimental results, the author was able to compare those with the numerical results and verify their accuracy. Half the model was used due to symmetry of the geometry, leading to a great reduction of cells and time. Layers of hexahedral cells are created near the moving parts, whereas the remaining stationary zones have tetrahedral elements. Using the remeshing, layering and smoothing capabilities of *Fluent*, a transient solution

is possible. The fluid used for the simulation is air whose density is calculated by the *ideal-gas-law* and the viscous model is *Standard* $\kappa - \varepsilon$. The species transport model is also activated in order to define 2 types of phases: burned and unburned. The intake boundary condition was defined by experimental results, by using a pressure profile in function of the crank angle.

The pressure interpolation was calculated by PRESTO!, the PISO algorithm was used for the pressure-velocity coupling method and the Second-Order Upwind Scheme was chosen for the discretization of all variables.

The results showed that the greater the engine speed the higher the cylinder pressure would be and at certain crank angles, due to greater exhaust pressure, backflow would occur. The author advises that improvement in the Algebraic Multigrid Method (AMG) solver is needed in order to enable simulations which use accurate fuel characteristics.

The study of IC engine combustion is, as well, a matter of great interest, as presented by [13] in an attempt to reduce emissions of a medium capacity two-stroke IC engine with stratified scavenging system. The validation of the obtained results was based on the outputs of a single two-stroke cylinder engine, with an alteration in the basic design by adding another port in the air supply system.

The model is created using *CATIA*, meshed by *Gambit* and exported to *Fluent*. The mesh possesses approximately 187000 elements. All three basic equations are solved (conservation of mass, momentum and energy); chemical analysis is also included in the analysis. The inlet and exhaust boundary conditions are defined as *velocity-inlet* and *pressure-outlet*, respectively.

The modification made to the engine improved performance, scavenging and trapping efficiencies, the last two being strongly affected by delivery ratio. The analysis also gave a reduction of Hydrocarbons (HC) emissions by 34-38% and Carbon Monoxide (CO) emissions by 22-25%

Other types of software are available to perform IC engine simulations, such is the case of [14], in which the authors use a *KIVA-3* code based numerical model to study a three-dimensional transient intake flow through a port-valve-cylinder system of a high-speed small motorcycle engine. Dynamic grid generation became the crucial point in order to perform the transient study, since piston and valves move, the mesh begins to stretch resulting in bad meshing and, consequently, bad results. Similarly to nowadays solution (in *Fluent*), a plane would be removed during the piston movement towards the Top Dead Center (TDC) and a ghost plane would be inserted when the piston moved towards the Bottom Dead Center (BDC). With this method, it was possible to do the same for the valve movement allowing an effective transient simulation. The intake boundary condition was assumed as *pressure-intake* and all walls had a *fixed-wall-temperature* condition.

Both velocity and pressure parameters were analyzed. During the intake process, shortly after the the intake valve opens, it is noticed that during a 40º crank angle gas enters the intake port from the cylinder. This occurs due to the pressure difference, which rapidly diminishes and by the time the valve is closed, pressure inside the cylinder is slightly greater than in the port.

The software used allows the user to perform transient IC engine solutions for both vertical and inclined valves and provided a good theoretical basis for optimizing engine port designs.

Different cases of IC engine analysis may require different approaches, as presented by [15]. Three engine simulations were performed in this study, in which results were compared with the respective simulation time: uni-dimensional, quasi-dimensional and CFD. The expansion cycle

of the high speed diesel engine was analyzed running under different motoring conditions and engine speeds.

The uni-dimensional showed to be very little time consuming, taking as long as 1 s to perform the simulation. It also calculated, with reasonable accuracy, the in-cylinder pressure; the same can not be said about in-cylinder mean gas temperature, which the software underestimates when compared to the other two models.

On the other hand, the quasi-dimensional analysis was capable of providing good results regarding local in-cylinder temperature distribution, as well as the qualitative effect of the cylinder geometrical design on in-cylinder flow and temperature, when compared to CFD results. With a computational time of 6 min, the quasi-dimensional model calculated the cylinder pressure more closely to the measured results than the uni-dimensional model. Additionally, the calculated heat transfer process through the cylinder walls is nearly the same as the CFD case results. The author concluded that this model may be useful as a preliminary study of the effect that the combustion chamber geometry has on the physical processes occurring within the cylinder, whereas the uni-dimensional model cannot perform this task since it does not take in account the design of the chamber.

The CFD model has greater capabilities of calculating detailed flow-fields for different engine designs as well as various physical processes, even though the calculation time was approximately 20 h.

For parametric cases, it was advised to perform a quasi-dimensional study first, in order to determine the limited number of cases of interest and then apply those cases on a CFD code for more detailed information.

As the previous case, CFD simulations of IC engines can be very time consuming, with some simulations taking months to complete. This is a problem for many entities, thus [16] developed a set of software tools, in order to reduce these simulation times, for IC engine flows and combustion. The author presents very good and detailed information on simulation setup, meshing and problems existent.

Chapter 2

Basic Theory of Internal Combustion Engine Analysis

2.1 Operating Characteristics

Every reciprocating engine, with the exception of the Wankel engine, operates in a similar way; the linear movement of a piston in a cylinder, due to confined and controlled explosions of a gaseous mixture, is transformed into rotational movement of the crankshaft which transmits the energy created by the explosion to a shaft and then to the components that generate vehicle motion. In order to obtain a fully functional engine, it is necessary to complete four steps: admission of a fresh mixture of fuel and air; compression of the charge in order for temperature and pressure to rise; explosion of the mixture, creating the energy needed to move the piston; and exhaust of the burned mixture.

Types of Ignition: Compression and Spark Ignition

The explosion of the mixture can occur in two distinct ways; by compression, also known as Compression Ignition (CI) and by external ignition or SI. In the first case, the gaseous mixture auto-ignites due to the rise of pressure and temperature during the compression stroke. The SI engine needs an external source, such as a spark plug, which, when near the TDC, releases a small electric charge to the mixture, igniting it.

Two-stroke & Four-stroke Cycles

There are two types of engine cycles: two-stroke and four-stroke. A stroke is the displacement of the piston from the TDC to the BDC and back. A cycle is completed after two strokes (one crankshaft revolution), meaning that in a two-stroke engine one cycle is necessary in order to conclude to entire process and in a four-stroke engine, two cycles are needed. The two-stroke can be explained with reference to Fig. 2.1.

1. Normally known as the *compression stroke*, the piston travels from the BDC to the TDC compressing the confined charge, which is sucked into the cylinder due to pressure difference. Usually, in this type of engine, the charge is mixed before entering the cylinder, also referred to as pre-mixed. However, if this is not the case, the fuel can be injected into the cylinder when the piston is near the TDC and, subsequently, the explosion occurs. In this stroke, two of the four necessary steps mentioned above are performed: compression and explosion;

2. The second phase is called the *power stroke*, in which the piston moves towards the BDC due to the rise of temperature and pressure. On the cylinder walls, there are cavities, called ports. These cavities are unveiled by the movement of the piston; as the piston descends, the exhaust port is uncovered, allowing the burned charge to escape. The

downward motion continues, revealing, afterwards, the inlet port, through which a fresh charge is allowed to enter. The last two steps are completed in this stroke: admission and exhaust. The process then restarts.

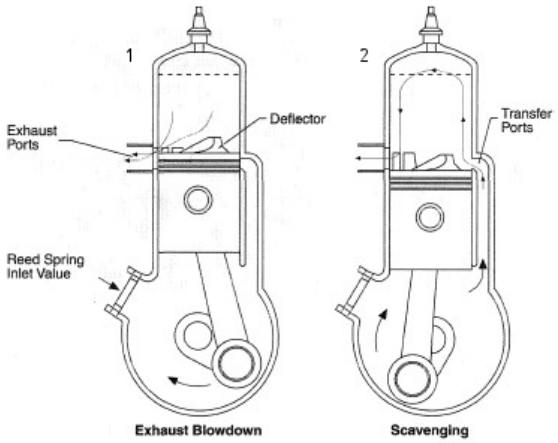

Figure 2.1: The two-stroke cycle stages: 1 - Compression Stroke; 2 - Power Stroke [17]

The four-stroke needs an extra revolution in order to complete the process. While the two-stroke engine performs two steps in one stroke, the four-stroke engine performs one step in each of its four strokes. Also, the gaseous mixture is controlled by a set of valves: the exhaust and admission valves. Normally, there is one of each; however, it is common to have more in recent engines. The process is as follows and is represented in Fig. 2.2.

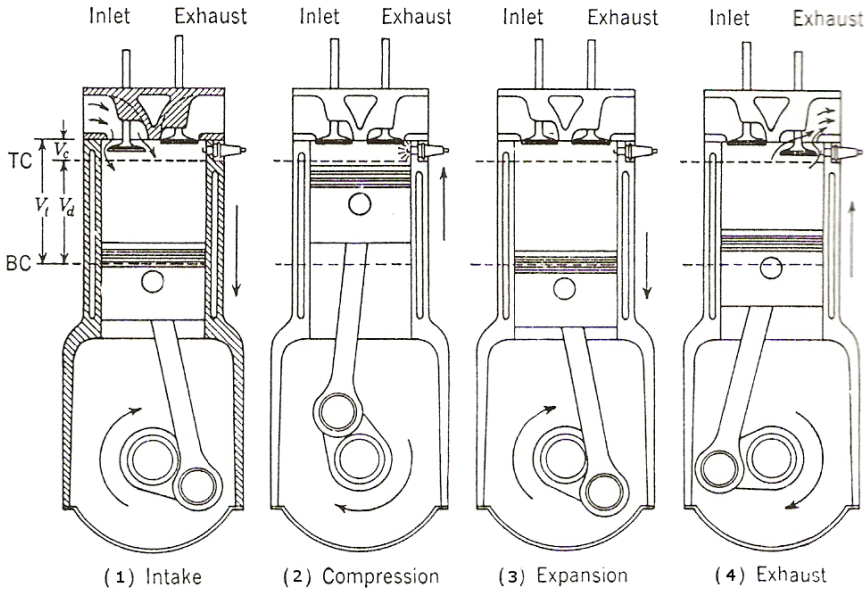

Figure 2.2: The four-stroke cycle stages [18]

1. With the piston at the TDC, the admission valve opens allowing the fresh charge into the cylinder. This happens due to the downwards movement of the piston, creating a difference in pressure and, consequently, a suction effect of the exterior air into the cylinder. This completes the first step: the *intake stroke*;

2. The following step is the *compression stroke*, in which, similarly to the two-stroke, the charge is compressed and the explosion occurs before the piston reaches the TDC;
3. After the explosion, the piston is pushed downwards towards the BDC, due to the increase of pressure and temperature. This is called the *power stroke*;
4. Finally, the piston moves upwards in order to expel the burned fumes caused by the explosion. The *exhaust stroke* thereby completes the full process.

Thermodynamically speaking, all four-stroke SI engines work on the Otto cycle, which is represented by the P-V cycle in Fig. 2.3. It is composed essentially of four internally reversible processes:

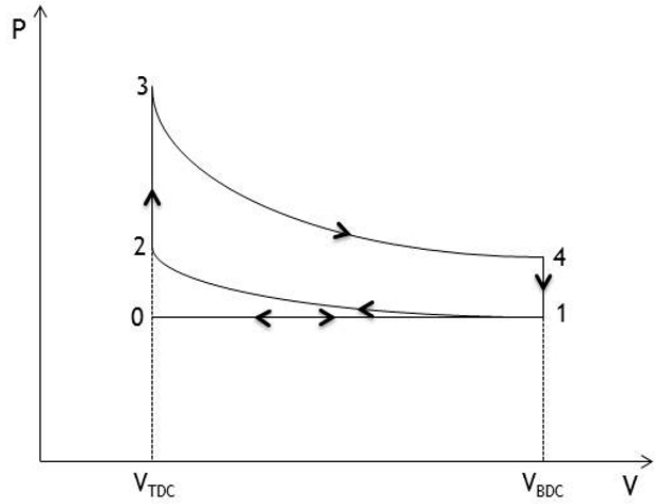

Figure 2.3: The Otto cycle

- 1-2 – Isentropic compression
- 2-3 – Constant volume heat addition
- 3-4 – Isentropic expansion process
- 4-1 – Constant volume heat rejection

There are two additional steps which do not appear in the theoretical Otto cycle [19]:

- 0-1 – Intake process
- 1-0 – Exhaust process

Fuels

Like any power unit, an IC engine requires a constant input of energy to produce work; this energy is extracted from the combustion of hydrocarbon fuels with air, during the process of converting chemical energy from the fuel into internal energy of the air molecules. Nowadays there are several fuels available, such as gasoline, diesel, crude oil and other derivatives, natural gas, Liquefied Petroleum Gas (LPG), propane, alcohol, methanol, ethanol and hydrogen. Carbon

and wood are solid fuels also widely used. From a more ecological point of view, biomass is becoming increasingly used due to the increase of fuel prices and environmental pollution.

Engine Parameters

During the process of an IC engine design there are several parameters and variables that should be considered in order to optimize its performance. Important factors, among others, are the dimensions of the engine, such as bore and stroke, which have a significant influence on the engine's overall performance and output.

For a given crank offset (a), the stroke (L) of an engine can be calculated by Eq. 2.1:

$$L = 2a \tag{2.1}$$

The bore-to-stroke ratio – Eq. 2.2 - is an excellent parameter to evaluate the engine's design. It usually has values in the range of 0.8 and 1.2, and offers a better insight of some parameters such as friction losses, thermal efficiency and piston speed. Connecting rod length-to-crank offset ratio (Eq. 2.3) is, as well, a recommended geometrical parameter to take into account, with values varying between 3 and 5, for small and medium engines, and 5 to 10 for larger engines.

$$\beta = \frac{B}{L} \tag{2.2}$$

$$R = \frac{r}{a} \tag{2.3}$$

Piston speed is also a factor not to be taken lightly; considering that the piston is accelerated and decelerated in each stroke, the material of the piston and connecting rod are subjected to incredibly high forces. Therefore, it is common to impose a safety limit in piston speed, varying between 5 and 15 m/s. Also, the gas flow within the cylinder suffers with the increase of piston speed; the higher the speed, the less time the intake and exhaust valves are open and subsequently, the mass flow rate must increase. Consequently, this may lead to an inability of the engine to introduce the necessary quantities of air in such a short time [20]. The average piston speed, considering a given engine speed (N), can be calculated by Eq. 2.4:

$$U_p = 2LN \tag{2.4}$$

For analytical purposes, it is useful to calculate the position of the piston (l) (Eq. 2.5) at a given crank angle (θ) and connecting rod length (r):

$$l = a\cos\theta + \sqrt{r^2 - a^2(\sin\theta)^2} \tag{2.5}$$

A very common performance indicator is the volume of displacement (V_d), presented in Eq. 2.6. In other words, the volume the piston dislocates from the BDC to the TDC.

$$V_d = \frac{\pi}{4} B^2 L \tag{2.6}$$

There is a remaining volume when the piston reaches the TDC which is called the combustion chamber or clearance volume (V_c). Therefore, the total volume of the cylinder when at the BDC is Eq. 2.7:

$$V_{BDC} = V_d + V_c \tag{2.7}$$

Eq. 2.8 shows the compression ratio (c_r), which is also an important parameter in IC engine design. CI engines have compression ratios in the range of 20 to 70, in extreme cases, while SI engines vary from 8 to 11.

$$c_r = \frac{V_c + V_d}{V_c} \tag{2.8}$$

Work, torque and power are three of the most important output parameters in any IC engine. Work is the result of pressure with the variation of volume; however, it is usually considered the Indicative Mean Effective Pressure (IMEP), also an excellent comparison parameter since it is independent of the size of the engine. Size is, in fact, associated to torque, whereas the speed of the engine is linked to power. IMEP is a measure of the indicated work done by the gas on the piston per unit of swept volume (Eq. 2.9):

$$IMEP = \frac{W_i \times N_c \times n}{V_d} \tag{2.9}$$

However, the Break Mean Effective Pressure (BMEP) presented in Eq. 2.10 is more relevant, since it is measured using a dynamometer and leads to a similar equation as Eq. 2.9:

$$BMEP = \frac{W_b \times N_c \times n}{V_d} \tag{2.10}$$

The ratio between these two pressures provides mechanical efficiency (Eq. 2.11):

$$\eta_m = \frac{W_b}{W_i} \tag{2.11}$$

Torque represents the ability of the engine to produce work and it is given by Eq. 2.12:

$$\tau = \frac{W_b}{n} \tag{2.12}$$

Finally, power is the rate at which the engine produces work and is calculated by Eq. 2.13:

$$P = 2\pi N \tau \tag{2.13}$$

The relation between the amount of air and fuel mixed together is perhaps the most challenging parameter in initial IC engine design. Therefore, Air-Fuel (AF) in Eq. 2.14 and Fuel-Air ratios (FA) in Eq. 2.15 are used in order to understand this process more easily.

$$AF = \frac{m_a}{m_f} = \frac{\dot{m_a}}{\dot{m_f}} \tag{2.14}$$

$$FA = \frac{m_f}{m_a} = \frac{\dot{m_f}}{\dot{m_a}} \tag{2.15}$$

The equivalence ratio offers a better insight into whether the mixture is too lean or rich. It is represented by relating the stoichiometric mixture with the actual one as shown in Eq. 2.16:

$$\phi = \frac{FA_{act}}{FA_{sto}} = \frac{AF_{sto}}{AF_{act}} \tag{2.16}$$

Due to emission issues and economic reasons, Specific Fuel Consumption (SFC) has become an increasingly important parameter in engine analysis and design. Eq. 2.17 offers a better insight into this matter.

$$SFC = \frac{\dot{m_f}}{\dot{W}} \tag{2.17}$$

Volumetric efficiency (η_V) relates the amount of air introduced into the cylinder with the actual capacity of the cylinder, presented by Eq. 2.18, and is one of the most important parameters in the characterization and modeling of four-stroke IC engines. The value of volumetric efficiency depends on several engine variables, such as engine speed, intake and exhaust manifold pressures and geometry of the system [21].

$$\eta_V = \frac{n\dot{m_a}}{\rho V_d N} \tag{2.18}$$

In theory, the mass of fresh charge in each cycle is equal to the product of air density evaluated at atmospheric conditions outside the engine and volume displaced by the piston. However, due to the short cycle time available and the existent flow restrictions, less than the theoretical amount of fresh charge enters the cylinder [22].

2.2 In-Cylinder Turbulence and Gas Motion

Characteristics of Turbulence

Turbulence is an important characteristic of fluid flows and it is largely present in many applications, especially in nature. Although the definition of turbulence seems easy and direct, it is rather difficult due to its complexity. Most view turbulence as a state of confusion and chaos, impossible to predict. This description is far from comprehensive. Peter Bradshaw then

presented a definition, which is considered by many as the most accurate and complete [23]:

"Turbulence is a three-dimensional motion dependent of time in which the stretching of vortices cause velocity fluctuations among all wave lengths, between a minimum set by viscous forces and a maximum set by the flows boundary conditions. It is the normal state of fluids, with the exception of low Reynolds numbers."

Due to turbulence, important transportation phenomena occur and the greater the intensity turbulence, the stronger transportation becomes. It is also essential for mixing in CI engines, since fuel and air are mixed separately and must be as homogeneous as possible.

Turbulence Equations

In order to perform an analysis on turbulence, a set of equations that govern this subject are necessary. Firstly, the Reynolds number indicates the ratio between inertial and viscous forces (Eq. 2.19).

$$Re = \frac{U \rho D}{\mu} \tag{2.19}$$

The Prandtl non-dimensional number relates the kinematic viscosity with the thermal diffusivity as shown in Eq. 2.20.

$$Pr = \frac{\nu}{\alpha} \tag{2.20}$$

Finally, the Navier-Stokes equations represent the complete condition of a fluid in motion, despite not having been completely solved yet (Eq. 2.21).

$$\begin{cases} \frac{Du}{Dt} = g_x - \frac{1}{\rho}\left\{\frac{\partial p}{\partial x} + \frac{\partial}{\partial x}\left[\mu\left(2\frac{\partial u}{\partial x} - \frac{2}{3}\nabla\cdot\vec{U}\right)\right] + \frac{\partial}{\partial y}\left[\mu\left(\frac{\partial u}{\partial y} + \frac{\partial v}{\partial x}\right)\right] + \frac{\partial}{\partial z}\left[\mu\left(\frac{\partial w}{\partial x} + \frac{\partial u}{\partial z}\right)\right]\right\} \\ \frac{Dv}{Dt} = g_y - \frac{1}{\rho}\left\{\frac{\partial p}{\partial y} + \frac{\partial}{\partial x}\left[\mu\left(\frac{\partial u}{\partial y} + \frac{\partial v}{\partial x}\right)\right] + \frac{\partial}{\partial y}\left[\mu\left(2\frac{\partial v}{\partial y} - \frac{2}{3}\nabla\cdot\vec{U}\right)\right] + \frac{\partial}{\partial z}\left[\mu\left(\frac{\partial v}{\partial z} + \frac{\partial w}{\partial y}\right)\right]\right\} \\ \frac{Dw}{Dt} = g_z - \frac{1}{\rho}\left\{\frac{\partial p}{\partial z} + \frac{\partial}{\partial x}\left[\mu\left(\frac{\partial w}{\partial x} + \frac{\partial u}{\partial z}\right)\right] + \frac{\partial}{\partial y}\left[\mu\left(\frac{\partial v}{\partial z} + \frac{\partial w}{\partial y}\right)\right] \frac{\partial}{\partial y}\left[\mu\left(2\frac{\partial w}{\partial z} - \frac{2}{3}\nabla\cdot\vec{U}\right)\right]\right\} \end{cases} \tag{2.21}$$

Where ∇ represents the gradient.

Two other very important turbulence characteristics are the kinetic turbulent energy and kinetic energy dissipation. Both have important roles in turbulence analysis (see Chap. 3).

The random characteristic of turbulence precludes the possibility of performing an analytical study; therefore it is necessary to use statistics, by resorting to parameters such as mean values and standard deviation.

Characteristics of In-Cylinder Turbulence

As will be seen throughout this chapter, turbulence is of extreme importance for overall performance since it affects combustion, mixture, heat transfer and evaporation. Turbulence is higher during intake, but then decreases as the flow rate declines near the BDC; it then increases during compression when near the TDC. The higher the engine speed, higher is the turbulence.

Types of In-cylinder Motion: *Swirl*, *Squish* and *Tumble*

During the engine cycle, the charge within the cylinder suffers several changes regarding turbulence. These modifications are beneficial for the overall performance of the engine, since they have great influence on the critical stages of compression and combustion. It has become clear that the intake process has a larger affect on these turbulent motions and may contribute greatly for higher turbulence intensity during the later stroke of compression, achieving this way faster burning rates [24].

Swirl is defined by Heywood as an organized rotation of the charge around the cylinder axis. Normally, *swirl* is formed by providing an initial angular momentum when entering the cylinder and prevails until the end of the power stroke. It is of great importance in both CI and SI engines: *swirl* provides a better and faster mixture of fuel and air in CI engines, while in SI engines *swirl* is fundamental for faster combustion [25].

Squish motion occurs by the end of the compression stroke, when the face of the piston is very near the cylinder head. It is characterized as a radially inward or transverse gas motion.

Finally, *tumble* is generated by *squish* motion, as a secondary rotational flow, rotating around a circumferential axis near the outer edge of the piston bowl.

2.3 Intake and Exhaust Flow

During the cycle of an engine, air and fuel must be induced, sealed and exhausted from the cylinder, in order to have a decent combustion. The mechanisms that allow these actions are called the *Intake* and *Exhaust Systems*. There are several important factors that can affect engine performance, with special attention given to volumetric efficiency. Among them are engine speed, valve area, lift, timing, compression ratio, mixture temperature and fuel to air ratio.

Intake System

The intake system consists of several components; however, this section will give greater emphasis to one particular component: the *intake valve*.

Air and fuel are fed to the cylinder through the intake manifold, which is a set of pipes, called *runners*. The mixture is then fed to each cylinder by activating the intake valve, which is normally driven by the camshaft at a regular pace, dependent on the engine speed. This happens because the valves are not constantly open: they open to receive the mixture into the cylinder,

close to seal the fresh charge and, by the end of the exhaust process, re-open to receive a new fresh charge and begin a new cycle.

There have been several types of intake valves, however, the most common in use is the poppet valve, mainly for being very inexpensive and having good seating and flow properties [26]. Nonetheless, there are other relevant valve types, such as the rotary and disc valves, and the sleeve valve, widely used in aero-engines.

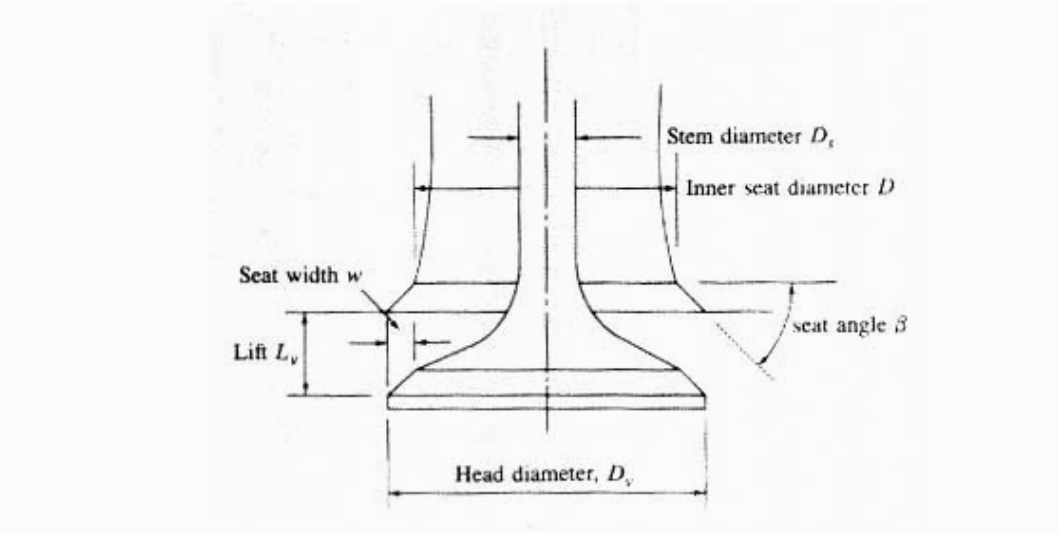

Figure 2.4: Components and dimensions of the poppet valve [25]

The valve or valve port are usually the greatest flow restriction during the intake process in an IC engine and has a major influence on volumetric efficiency. Volumetric efficiency, mentioned in Sec. 2.1 , is one of the most important factors when discussing intake. As seen in Eq. 2.18, volumetric efficiency is directly proportional to flow rate, therefore the intake system must be capable of supplying the sufficient air in order to improve cylinder filling. Although this parameter cannot reach 100%, due to the addition of fuel, there are several factors that can increase its value to a desired maximum:

- Engine speed limits the time the intake valve is open; however, contrarily to common sense, maximum volumetric efficiency is not achieved at lower engine speeds, but at a mid-range speed.
- The type of fuel and how and when it is added to the intake air is also relevant. If added to early, despite improving the mixture, since the fuel has more time to evaporate, it lowers volumetric efficiency due to displacement of air caused by the addition of evaporated fuel. The opposite happens when fuel is added later on in the process.
- Intake temperature affects the air density by lowering its value. Normally, the intake manifold has a greater temperature than the surrounding air in order to assist fuel evaporation. However, by doing so, it reduces volumetric efficiency. At lower engine speeds, this factor increases.
- When both valves, intake and exhaust, are open simultaneously, valve overlap occurs. This event will be discussed later on.

- The time of closure of the intake valve will also affect volumetric efficiency and will also be discussed later on.

SI engines normally have lower volumetric efficiencies due to most of these factors, when compared to CI engines.

Valve design should be given much care due to its importance regarding volumetric efficiency and reducing pressure drop. Air flow into the cylinder is mainly dependent on port area; larger valves allow higher air flows. Therefore, in some cases more than one intake valve is installed even though this leads to greater complexity of the intake system. Despite this fact, the enhancement of volumetric efficiency is viewed as the prime goal in this matter. The area through which the flow passes is a matter of great importance, no matter how big the challenge. The mass flow rate through the poppet valve is usually described as a compressible flow through a flow restriction as presented in Eq. 2.22.

$$\dot{m} = \sqrt{\frac{C_D A_R p_0}{\sqrt{RT_0}} \left(\frac{p_T}{p_0}\right)^{\frac{1}{\gamma}} \left\{\frac{2\gamma}{\gamma - 1}\left[1 - \left(\frac{p_T}{p_0}\right)^{\frac{\gamma-1}{\gamma}}\right]\right\}} \tag{2.22}$$

Where the discharge coefficient is calculated by Eq. 2.23:

$$C_D = \frac{A_{act}}{A_{cur}} \tag{2.23}$$

in which the valve curtain area is:

$$A_{cur} = A_R = \pi D_v L_v \tag{2.24}$$

The choice of reference area is not universally defined; however, the most convenient and used is Eq. 2.24 . Since intake valves are the greatest restriction when it comes to air flow, it is common to consider a minimum intake area, which is given by Eq. 2.25, for preliminary reasons:

$$A_{min-in} = CB^2 \frac{U_{P_{max}}}{c_{in}} \tag{2.25}$$

where:
C = constant, normally considered 1.3.

For high engine speed situations, if the port area is not large enough, the induced flow may choke. In other words, the flow at the smallest port area may reach sonic speed and compromise volumetric efficiency greatly. In this case, an inlet Mach index is often used, represented as follows in Eq. 2.26, where for $Z \geq 0.5$, volumetric efficiency decreases rapidly:

$$Z = \frac{A_P U_P}{C_i A_i c} \tag{2.26}$$

$C_i A_i$ is the average effective open area of the valve - $C_D \pi D_v L_v$.

Mach number correlates volumetric efficiency better than the Mach index, therefore an alternative can be considered by using Eq. 2.27:

$$M = \frac{U}{c} \tag{2.27}$$

It is possible to relate both Eq. 2.26 and Eq. 2.27 and obtain:

$$M = \frac{Z\left(\frac{\eta_V}{100}\right)180}{\theta_{IVC} - \theta_{IVO}} \tag{2.28}$$

Valve lift is the distance at which a valve opens and has a major influence on induced flow. If the distance is too short at mid-range and high speeds, air flow is restricted; above a critical value, lift no longer has a significant influence on the effective valve opening area. Discharge coefficient, when based on the valve curtain area, is a non-continuous function which is related to valve lift and valve diameter ratio; this ratio has a typical maximum value of 0.25.

The intake valve usually begins to open at approximately 10º to 25º before the TDC. Although engine performance is quite insensitive to this timing point, it is important to consider two objectives: the valve should be at its maximum lift at the TDC in order to get the most of the intake stroke and to avoid that in-cylinder pressure does not plunge too early during the intake stroke. Closing, on the other hand, is more important since it defines the quantity of air that ends up being induced into the cylinder. It usually occurs between 40º to 60º after the BDC and this happens, as mentioned earlier, to improve volumetric efficiency, given that at the beginning of the intake stroke, pressure within the cylinder is less than the intake manifold pressure. As the piston moves towards the BDC, air is induced into the cylinder due to the vacuum created by the additional volume being displaced. When the piston reaches the BDC, this pressure difference still exists, thus the optimum closing time would be when the cylinder and the intake manifold pressure are equal. It is important to notice that valve timing can only be optimized for one engine speed only. In order to optimize a large range of speeds, it would be necessary to resort to valve-timed controllers. At low engine speeds, backflow may occur, depending on intake valve closing. Backflow is when the induced charge flows back to the admission port, causing volumetric efficiency to decrease.

When the intake valve begins to open, three types of flow characteristics usually occur:

- At low-lift, the flow remains attached to both valve head and valve seat;
- At intermediate-lift, the flow separates from the inner edge of the valve head;
- And at high-lift, the flow separates from the valve seat wall.

Factors that influence the performance of the intake valve assembly are valve seat width, valve seat angle, which at low-lifts can affect the discharge coefficient, valve cone angle, rounding of the corners of the valve seat, reducing the tendency for the flow to separate and, therefore, increase discharge coefficient at higher lifts, and port design. Annand and Roe et al. 1974 concluded that the desirable valve seat angle would be 30º with a minimum width and an upper surface angle of the valve head of about 10º [27]. The cone angle has its influence on intake flow as well, where a 0º cone angle is desired [28]. Also, it was found that elliptical cross sectional inlet ports are more conductive to generate tumble motion during the intake process [29].

Exhaust System

After combustion and using the burned gases to transfer work to the crankshaft during the expansion stroke, these same burned gases must be expelled from the cylinder to allow a new and fresh charge in. The exhaust system is responsible for this event and can be analyzed in two different moments: *blowdown* and *exhaust stroke*.

Blowdown occurs near the end of the power stroke, when the exhaust valve opens at approximately 60º to 40º before the BDC. At this point, both pressure and temperature of gas within the cylinder are very high, 3 to 4 atm and 1000 K respectively, and, in the exhaust system, pressure is practically 1 atm. When the valve opens, differential pressure causes an abrupt flow from the cylinder through the valve. Normally, at first, the flow will choke due to the high temperature of the inner gas, therefore increasing the speed of sound. As the flow leaves the cylinder, it experiences a drop in pressure and temperature due to expansion cooling, and by the end of the power stroke, the gas will have lower velocity and kinetic energy.

Following *blowdown* is the exhaust stroke. As the piston reaches the BDC, the exhaust stroke begins, in which the piston pushes the burned gases through the open exhaust valve. During this motion, it is considered that the pressure is constant at a value not much higher than the exhaust system pressure, with the greatest pressure drop occurring at the valve. By the end of this process, all the burned gases are expected to have been expelled from the cylinder; however, this does not happen mainly due to the limited time it takes in order to close the exhaust valve. The camshaft is designed in such a way that valve closing is as smooth as possible to mitigate other problems such as noise and wearing. If designed to close earlier, it would have to start closing before reaching the TDC, which is not desirable since the exhaust stroke will not have been completed. Consequently, when the exhaust valve closes, a residual of burned gases remains in the clearance volume, since the piston cannot push any further and the pressure difference is minimum. The exhaust valve then closes after the TDC between 8º and 20º, but can go up to 60º for high engine speeds.

This leads to another issue called *valve overlap*. As mentioned in the intake system, the intake valve starts to open between 10º to 25º before the TDC, meaning that both intake and exhaust valves will be open simultaneously for a brief amount of time defined by the exhaust valve closing. The main problem in this situation is reverse flow of the exhaust gases into the intake system, contaminating the incoming fresh charge, therefore leaving more exhaust residuals for the next cycle. At low engine rotations, this situation aggravates and in idle conditions it worsens, since in these conditions the time of overlap is longer. Another unwanted consequence is the non-evaporated fuel from the mixture going directly to the exhaust port, causing excessive pollution.

Exhaust valves are normally smaller than intake valves; yet these should be as large as possible since the same amount of mass flows through both intake and exhaust ports. This allows later exhaust valve opening and a longer expansion stroke, and consequently takes full advantage of output work. Similarly to the intake system, the minimum exhaust valve area can be approximated by Eq. 2.29:

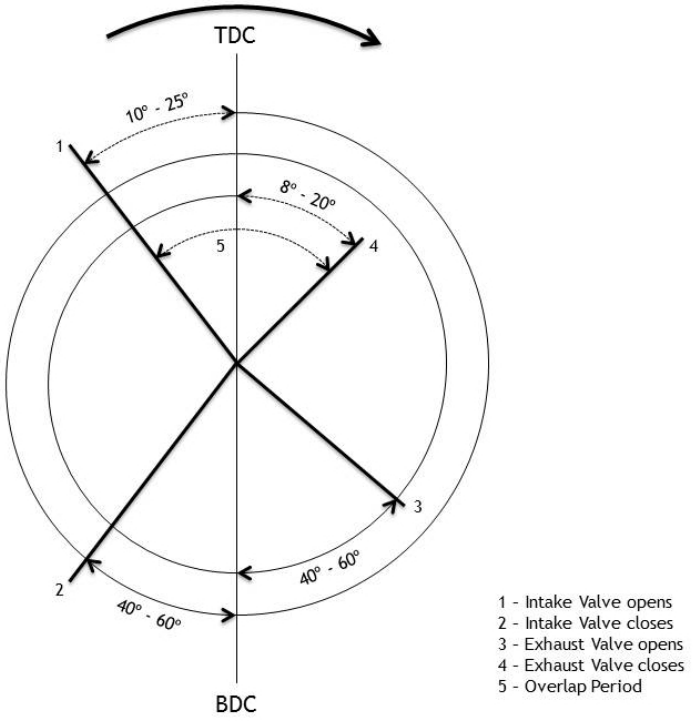

Figure 2.5: Valve timing diagram

$$A_{min-ex} = CB^2 \frac{U_{P_{max}}}{c_{ex}} \tag{2.29}$$

For comparison reasons, the intake and exhaust areas can be related by Eq. 2.30:

$$\alpha = \frac{A_{min-ex}}{A_{min-in}} \tag{2.30}$$

where α normally varies between 0.8 and 0.9.

Exhaust gases suffer great temperature variations when leaving the cylinder. On average, they can reach between 700 K and 900 K; when in idle, 600 K and 700 K; and at maximum power, 1100 K. During the exhaust process, the gas will reach its highest temperature still in the cylinder, which will gradually decrease throughout the exhaust valve and exhaust system. Along with temperature, mass flow varies greatly as well due to *blowdown* and the fact that the exhaust valve restricts the flow.

In comparison with the intake valve, exhaust valve lift has much less impact on the discharge coefficient, even though pressure ratio is much greater in the exhaust valve. Therefore, the design of the exhaust valve is less critical than the admission valve, and the seat angle should be between 30º and 45º.

Chapter 3

Numerical Modeling and Planning

3.1 Governing Equations

The area of fluid dynamics studies the interactive motion of a great amount of individual fluid particles, such as molecules or atoms. In order to use fluid dynamics as a tool in R&D, it is necessary to consider that the fluids' density is high enough to be approximated as a continuum. The word *continuum* implies that the fluid will contain a sufficient number of particles to study, even at infinitesimal small volumes, which makes it possible to calculate and define fluid properties, such as temperature, pressure, density and velocity [30].

The pillars of fluid dynamics are a set of governing equations that, when implemented, allow the user to assume certain conditions and, consequently, simplify the complexity that surrounds fluid motion: the conservation laws. The conservation of a defined flow quantity denotes that the total variation of an arbitrary volume can be expressed as the net effect of the amount of the quantity being transported across the boundary of the volume. The amount of quantity crossing the boundaries is called *flux* and can be decomposed into two components: *convective* and *diffusive transport*. The conservation laws used are [31]:

- Conservation of Mass or Continuity - defines that mass cannot be created nor destroyed, which leads to the conclusion that any variation of mass would imply a shift of fluid particles.

$$\frac{\partial p}{\partial t} + \frac{\partial pu}{\partial x} + \frac{\partial pv}{\partial y} + \frac{\partial pw}{\partial z} = 0 \tag{3.1}$$

- Conservation of Momentum - Newton's 2nd Law of Motion is applied in the momentum equation, which states that any variation in momentum is due to the net force acting on a mass element. These forces can be of two types: *body forces* and *surface forces*. The first component acts externally on the mass of volume, such as gravitational, Corioles and buoyancy forces; the second set of forces derive merely from pressure and shear and normal stresses. By adding up all of the mentioned contributions we obtain Eq. 3.2 in the differential form for all three components (x, y and z), respectively.

$$\begin{cases} \rho g_x + \dfrac{\partial \sigma_{xx}}{\partial x} + \dfrac{\partial \tau_{yx}}{\partial y} + \dfrac{\partial \tau_{zx}}{\partial z} = \rho \left(\dfrac{\partial u}{\partial t} + u\dfrac{\partial u}{\partial x} + v\dfrac{\partial u}{\partial y} + w\dfrac{\partial u}{\partial z} \right) \\ \rho g_y + \dfrac{\partial \tau_{xy}}{\partial x} + \dfrac{\partial \sigma_{yy}}{\partial y} + \dfrac{\partial \tau_{zy}}{\partial z} = \rho \left(\dfrac{\partial v}{\partial t} + u\dfrac{\partial v}{\partial x} + v\dfrac{\partial v}{\partial y} + w\dfrac{\partial v}{\partial z} \right) \\ \rho g_z + \dfrac{\partial \tau_{xz}}{\partial x} + \dfrac{\partial \tau_{yz}}{\partial y} + \dfrac{\partial \sigma_{zz}}{\partial z} = \rho \left(\dfrac{\partial w}{\partial t} + u\dfrac{\partial w}{\partial x} + v\dfrac{\partial w}{\partial y} + w\dfrac{\partial w}{\partial z} \right) \end{cases} \tag{3.2}$$

- Conservation of Energy - the 1st Law of Thermodynamics is the fundamental principal applied in the energy equation by stating that any changes of total energy within the volume are caused by the rate of work of the forces acting on the volume, as well as the heat flux through its boundaries. The resulting equation is shown in Eq. 3.3 in terms of total energy (e).

$$\begin{aligned}\frac{\partial}{\partial t}\left[\rho\left(e+\frac{U^2}{2}\right)\right]+\nabla\left[\rho\left(e+\frac{U^2}{2}\vec{U}\right)\right] = \rho\dot{q}+\frac{\partial}{\partial x}\left(k\frac{\partial T}{\partial x}\right)+\frac{\partial}{\partial y}\left(k\frac{\partial T}{\partial y}\right)+\frac{\partial}{\partial z}\left(k\frac{\partial T}{\partial z}\right)\\ -\frac{\partial(up)}{\partial x}-\frac{\partial(vp)}{\partial y}-\frac{\partial(wp)}{\partial z}\\ +\frac{\partial(u\tau_{xx})}{\partial x}+\frac{\partial(u\tau_{yx})}{\partial y}+\frac{\partial(u\tau_{zx})}{\partial z}\\ +\frac{\partial(v\tau_{xy})}{\partial x}+\frac{\partial(v\tau_{yy})}{\partial y}+\frac{\partial(v\tau_{zy})}{\partial z}\\ +\frac{\partial(w\tau_{xz})}{\partial x}+\frac{\partial(w\tau_{yz})}{\partial y}+\frac{\partial(w\tau_{zz})}{\partial z}+\rho\vec{f}\cdot\vec{U}\end{aligned} \tag{3.3}$$

By combining Eq. 3.1, 3.2 and 3.3, we obtain the complete Navier-Stokes equations (Eq. 2.21).

3.1.1 Spatial and Time Discretization

The great number of numerical methods available for the Navier-Stokes solution led to a separate discretization in space and time, called the *method of lines*. This method makes it possible to use the grid to construct control volumes and evaluate the flux integrals or to approximate the spatial derivatives of the flow quantities, depending on the chosen algorithm. Furthermore, the time-dependent equations are calculated after an initial solution is found. This approach allows the selection of different kinds of approximations for both convective and viscous fluxes, as well as for time integration.

Spatial Discretization

To solve the governing equations and calculate the desired flow variables, the space in which the flow is to be computed (physical space) must be divided into a great number of grid cells. This is called *grid generation* or *mesh* [32].

The mesh can be either structured or unstructured. In the first case, quadrilaterals (2D) or hexahedra (3D) are used. The main advantages of this type of grid is the computer memory access, which means that, due to the identification system employed to each cell, accessing the neighbors of a grid point is much faster and easier. However, in complex geometries implementing structured meshes is quite difficult. For this reason, unstructured meshes are used in which triangular (2D) and tetrahedral (3D) cells are created. This type of structure provides greater flexibility and is faster to build when compared to the structured grid. In some cases, it is common to use a mixed grid, in which both triangles and quadrilaterals (2D) or tetrahedra and hexahedra (3D) are used, making it possible to reduce geometrical cell count.

Independently of the type of mesh used, it is very important to verify that there are no gaps between the grid cells and they should not overlap. These issues may lead to improper compu-

tation or even grid errors. Additionally, the mesh should be as smooth as possible, since abrupt changes in the volume of individual cells or stretching ratio may affect the quality of the overall grid and, consequently, lead to inaccurate results. The accuracy of the results will also depend on mesh size, where a refined mesh will give a better output than a coarser one, with the cost of time and computer resources.

Furthermore, special discretization schemes are implemented in order to calculate flow variables. These schemes are widely used in computational simulations, both fluid and structural [33]:

- Finite Difference Method - employs a Taylor series expansion of the derivatives of the flow variables. It is known for its simplicity, high order approximations and accuracy. However, the grid must be structured and this restricts its use. Thus, nowadays the finite difference method is rarely used, being applied to simple geometries and, at times, in Direct Numerical Simulation (DNS) of turbulence.

- Finite Volume Method - directly uses the integral form of the Navier-Stokes equations. This method divides the physical space in an arbitrary number of polyhedral control volumes. The control volumes can be defined in two distinct ways: Cell-Centered scheme and Cell-Vertex scheme. The first case stores the flow variables in the center of the grid cell, thus the control volume is identical to the grid cell. The second scheme stores the flow variables at the grid points. The advantage of this method over the previous one is that the spatial discretization is done directly in the physical space, avoiding problems that could emerge from the transformation of coordinate systems. In addition, the finite volume method is much more flexible when compared to the finite difference method, being easily used with structured or unstructured meshes. Moreover, this method has the ability to correctly compute weak solutions of the governing equations, which are essentially solutions that are usually poorly calculated.

The numerical schemes used to perform the spatial discretization, for both methods mentioned, are of two types.

- Central Schemes - this scheme's principle is to estimate the conservative variables to the left and to the right of the control volume, thus to evaluate the flux near it. Little CPU time usage is a great advantage when compared to the *Upwind Schemes*.

- Upwind Schemes - greater ability to capture discontinuities and capable of solving boundary layers with much less grid points. However, in second or higher orders, spatial discretization accuracy is largely affected, since limiters need to be employed to prevent oscillations near strong discontinuities. These limiters are known for stalling the convergence and increasing the computational effort.

Time Discretization

As both spatial and time variables are decoupled, it is possible to discretize each independently and therefore, time discretization can be calculated either before or after spatial discretization. The choice of the time-stepping scheme is very relevant and can influence the results for a given problem depending on whether one wishes to have a time accurate discretization, in the case of

highly dynamic flows, or to match the numerical solution to a steady state, by giving an initial guess.

Time discretization is mainly divided into two methods - *Explicit Scheme Method* and *Implicit Scheme Method*.

The first method presents the issue of not being necessarily stable, which means that the time-step cannot be chosen arbitrarily. There are two stability variables that make it possible to analyze whether the discretization will stabilize or not: they are the Courant (Eq. 3.4) and the Diffusion numbers (Eq. 3.5), which, in order to assess if there is or not stability, should meet a set of criteria (Eq. 3.6), Courants and von Neumann. Nonetheless, the fact that each variable can be solved directly from known values with low cost per time step is a great asset for this method.

$$C = \frac{U\delta t}{\delta x} \tag{3.4}$$

$$\beta = \frac{\alpha\delta t}{\delta x^2} \tag{3.5}$$

$$\begin{cases} C < 1 \\ \beta < \frac{1}{2} \vee C < 2\beta \end{cases} \tag{3.6}$$

The implicit scheme method, however, is much more stable in a wide range of time-steps and has excellent iterative solvers for steady-state problems. This leads to higher computational cost per time-step and the fact that the discretization equation cannot solve each variable for each time-step directly because three unknown variable remain. Due to this issue, it is more difficult to implement this method. Additionally, with the increase of the time-step, the convergence of the linear solvers deteriorates.

Due to the extent of this matter, it is advised to see the recommended references.

3.2 Turbulence Models

Inviscid and laminar flows are rather simple and direct when it comes to calculate flow variables and do not raise any fundamental issues. Turbulent flows, in the other hand, are much more complex and demand a different approach. As seen previously in Sec. 2.2, turbulence is known for its random behavior and difficult to predict; therefore, models are created. These models should be chosen carefully depending on the simulation in hand, since one model can be accurate in one situation and be completely inaccurate in another.

Several main models known and widely used in engineering will be presented in this section and explained, in order of descending computational demand.

The DNS applies the time-dependent Navier-Stokes equations directly. Technically, DNS can solve every fluctuating motion in the fluid; however, even with the most advanced supercomputers, it demands too much time and computational resources. The scale of the spatial resolution is around $Re^{9/4}$ and CPU time would be approximately Re^3, which even for high performance computers is very demanding. With the increase of the Reynolds number, the grid must be finer and the time step smaller. Nevertheless, it is possible to calculate simple flow cases at very low Reynolds numbers and DNS is a very important tool for understanding turbulent structures as well as laminar turbulent transitions. It also has an important role in the development and calibration of new or improved turbulence models.

Large Eddy Simulation (LES), as the name leads to believe, is based on the fact that small scales of turbulence have more characteristics than the larger ones, which carry the turbulent energy. Thus, LES calculates the large scale *eddies* with great accuracy and later on approximates the effects caused by the smaller *eddies*. Even though LES demands less grid points and, therefore allows higher Reynolds numbers, it still demands very high computational processing and small time steps, as well as it can be unstable in certain situations due to its three dimensional analysis. The reason why LES is rarely applied in IC engines is due to complications introduced by compressibility, complex cylinder geometries, moving boundaries, turbulence and combustion interaction difficulties [34]. Nevertheless, engineering would highly benefit from this tool, especially in cases where great detail is needed in complex flows, such as large scale mixing, combustion chambers and engines, heat transfer, rotary flows, aerodynamic noise and large separated unsteady flows.

Currently, the most used CFD tool among engineers is based upon the *Reynolds-Averaged Navier-Stokes* (RANS) model. RANS is based in the decomposition of the flow variables into mean and fluctuating parts following by time or ensemble averaging. When decomposed, the flow variables are inserted in the Navier-Stokes equations, obtaining basically the same equations for the mean variables. However, two additional terms are added to the equations: the *Reynolds-stress tensor* (Eq. 3.7) is added to the tensor of viscous stress, which represents the transport of the mean momentum due to turbulent fluctuations; the *turbulent heat vector* enhances the diffusive heat flux. Both of these terms require a model each.

$$\tau_{ij} = \rho\overline{u_i^{'}u_j^{'}} \tag{3.7}$$

When compared to the previous models, RANS requires considerably less computational power due to the coarser meshes. This factor is the reason why RANS is greatly used in engineering applications. However, due to the use of means, little detail can be obtained from the turbulent structures.

In order to close the RANS equations, several turbulent models were created and fall into two categories: the *Eddy Viscosity Models* (EVM) and the *Reynolds Stress Models* (RSM).

EVM assumes that the stress is proportional to the velocity gradient and leaving only a new unknown quantity needed - effective turbulent viscosity (μ_t). Being the most used in engineering, it has its limitations: isotropy is automatically assumed, despite many flows possess Reynolds stresses highly anisotropic; does not include the Reynolds stresses factor on the rate of flow ro-

tation; and EVM assumes that the Reynolds stress always scales with the strain rate tensor of the mean velocity, which is not always valid. The following section presents most of the RANS based models available (in *ANSYS Fluent*). They are presented in ascending computational demanding.

- *Spalart-Allmars* (SA) - a low cost, one-equation RANS model, capable of solving the transport equation for modified eddy viscosity. SA was designed mainly for aerospace purposes, particularly wall-bounded flows, boundary layer flows and supersonic/transonic flows over airfoils. Despite its good results for boundary layers subjected to adverse pressure gradients, it lacks accuracy predicting the decay of homogenous, isotropic turbulence.

- *Standard* $\kappa - \varepsilon$ - the versatility of this model along with its robustness and reasonable accuracy in several applications, awards the $\kappa - \varepsilon$ model as the most used in engineering applications [35]. Besides turbulent situations, it offers as well sub-models for combustion, compressibility and buoyancy, among others. It is based by solving the equation for turbulent energy (κ) and dissipation rate (ε) (a two equation model), which then together results in eddy viscosity. The main limitations present in this model are inaccuracy in predicting spreading rate of round jets, poor performance in flows which present very large pressure gradients, strong separation, high swirling component and large streamline curvature. The model parameters used are obtained through benchmark experiments data.

- *Realizable* $\kappa - \varepsilon$ - the mode through which the dissipation rate is calculated in this model greatly differs from the Standard $\kappa - \varepsilon$ model. It provides slightly more performance than the previous model, mainly in the applications mentioned for the Standard $\kappa - \varepsilon$.

- *Re-Normalization Group* (RNG) $\kappa - \varepsilon$ - the equations are derived analytically, contrarily from the two previous models. Has better performance than the Standard $\kappa - \varepsilon$ in complex shear flows, high strain rates, swirl and separation flows.

- *Standard* $\kappa - \omega$ - also widely used in aerospace applications, however with improved behavior under adverse pressure gradients and more sensitive to free-stream conditions. Similarly to the Standard $\kappa - \varepsilon$, it has as well several sub-models such as compressibility effects, transitional flows and shear-flow corrections.

- *Shear Stress Transport* $\kappa - \omega$ - possesses a particularly useful tool which gradually transitions from the Standard $\kappa - \omega$ model near the wall to higher Reynolds numbers of the Standard $\kappa - \varepsilon$ model beyond the boundary layer.

RSM is a far more complex, but flexible second-closure model. It derives the Reynolds stress components by averaging the products of velocity fluctuations and Navier Stokes equations. Despite created to avoid the problems that emerged from the EVM, not always does the RSM provide better results [36] [37].

The *Algebraic Reynolds Stress* (ARS) is similar to the RSM and uses two equations as well. However, due to numerical issues that arise from both these models, first-order closures are preferred.

3.3 Model Construction

In the process of assembling a numerical simulation, several steps are taken in order to accurately predict the outcome of the simulation. Among these steps are the model dimensioning, construction and meshing which will be presented in this section.

3.3.1 Geometry

The engine used as reference for this study is the two-stroke OP engine, Jumo 205E. Transforming a two-stroke OP engine into a four-stroke leads to some issues, as presented in Chap. 1, such as the location of the intake and exhaust valves. Few options are available for their location and at a first glance, the most reliable is a *flathead* or "L-head" configuration.

During the 1950's, the *flathead* engine was widely used, however rapidly became obsolete when the valve system of the IC engine underwent significant changes [38], giving place to the conventional overhead valve engine. Today, the *flathead* engine is used in small displacement engines, such as lawn mowers, electric generator power systems, snowblowers, weed trimmers, lawn edgers, go kart motors and so on. Nevertheless, the *flathead* engine is still one of great interest and several ideas have been presented in order to make it more competitive with the overhead valve engine [39].

The most notable difference of the *flathead* engine to the overhead valve engine is the location of its valves. As seen in Fig. 3.1, both valves are located parallel to one side of the cylinder, which allows a more compact design of the engine [40]. Not having both valves facing the piston brings one particular advantage: more freedom regarding valve timing and lift. However, the piston has very little direct contact with the combustion chamber, which can lead to a non-uniform combustion since the flame does not spread over the entire interior of the cylinder bore [41]. Another disadvantage of the *flathead* engine is the poor air flow characteristics during both intake and exhaust strokes, greatly due to the rough air flow path (corners and flat surfaces) [42].

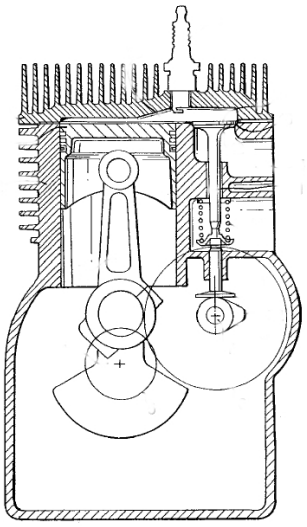

Figure 3.1: Schematics of the *flathead* engine (adapted from [40])

With the *flathead* concept in mind, there are two components which need dimensioning: both valves and the combustion chamber. Both valves are dimensioned based on the information displayed in Sec. 2.3 and on other large engines. The combustion chamber must be dimensioned in a way that it can accommodate both valves, allow their respective lift and simultaneously maintain the compression ratio to a pre-defined value. The dimensions of the model in study is presented in Tab. 3.1, as well as other information required for the simulation, and information about the Jumo 205E is presented in App. A. Hence that the compression ratio of the model engine has been reduced in order to adapt it to function as a SI engine. The remaining parameters, such as bore and stroke, are the same as the engine of reference. Both piston heads are chosen to be flat-crowned [43].

Table 3.1: Model engine dimensions

Parameters	
Bore	105 mm
Stroke	160 $mm \times 2$
Compression Ratio	10
RPM	2500 rpm
Intake Valve Diameter	65 mm
Intake Valve Lift	13 mm
Intake Valve Seat Width	2 mm
Intake Valve Seat Angle	30º
Exhaust Valve Diameter	59 mm
Exhaust Valve Lift	13 mm
Exhaust Valve Seat Width	2.5 mm
Exhaust Valve Seat Angle	45º
Clearance Height	15 mm
Gap	0.2 mm

The design of the model (Fig. 3.2) is done by resorting to the *Part Design* tool of *CATIA V5 R19* software. It is recommended that the model is at the TDC position with both valves closed. For meshing reasons, a gap is placed between the valves and their respective seats as shown in App. B.1. More detail of the geometry is presented in App. B.2. Initially, only half of the geometry was considered, in order to reduce computational cost, however, due to a reported *bug* in the software, this had to be reconsidered and the whole domain was used. The motive of this alteration is explained further in the text.

The final stage of this process is the decomposition of the geometry. When using the *ANSYS Internal Combustion Engine Workbench*, the decomposition is done automatically for conventional overhead valve engines, however for different configurations it may be more complicated, as is the case, and requires to be done manually. After importing the geometry to *ANSYS Design Modeler* in IGES format, the model will be split into several domains, as recommended by *ANSYS* for IC engine simulations [44]. Firstly, all solid bodies are removed, which in this case is only the intake and exhaust valve. Afterwards, two bodies are created: the *inboard* and the *vlayer*. The *inboard* is a cylinder shaped body which will surround the curvilinear area of the valve intended to prevent great mesh deformations during the simulation. The *vlayer* is a layer with the thickness of the gap created which covers the valve's upper surface and has the same intentions as the *inboard*. By the end of the decomposition there will be a total of 8 domains (see App. C).

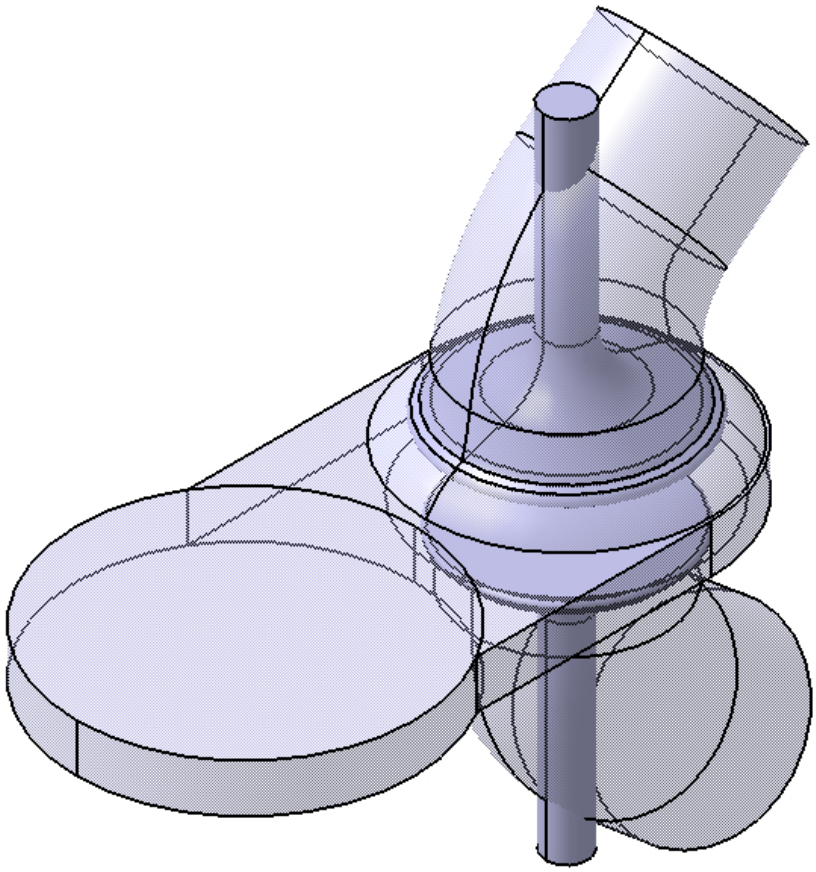

Figure 3.2: Domain of the model engine and valve bodies

3.3.2 Generation of the Numerical Mesh

The mesh generation is possibly the most important step during the construction phase of the model, since a good mesh is more likely to provide with better and trustful results. The software used for this step is *ANSYS Meshing*.

The cylinder, *inboard* and *vlayer* zones have structured meshing, whereas the chamber and ports have an unstructured type. The mesh size for each zone can be calculated with use of a *Reference Size* (RS) (Eq. 3.8).

$$RS = \frac{2\pi \frac{D_v}{2}}{100} \tag{3.8}$$

From this reference size, a minimum and maximum mesh size can be defined ($\frac{RS}{3}$ and $3RS$, respectively) as well as the *vlayer*, *inboard* and chamber mesh size ($\frac{RS}{4}$, $\frac{2}{3}RS$ and RS, respectively) [45]. Due to divergence reasons, the mesh size is chosen differently from the previous suggestion (see Tab. 3.2).

The resulting mesh has a total of 933294 nodes and 3638149 elements and is displayed in detail in App. D. The number of elements will increase with the movement of the pistons during the simulation. Among the available mesh quality parameters, orthogonal quality and mesh skewness are of great importance. Tab. 3.3 and 3.4 present the spectrum of these parameters,

Table 3.2: Mesh sizing values

Mesh	**Size Value** [mm]
Min. Mesh Size	0.2
Max. Mesh Size	2
Vlayer Size[1]	0.5
Inboard Size[1]	0.5
Chamber Size	1
Cylinder Size	2
Admission and Exhaust Ports	2
Interface between the Chamber and *vlayers*[2]	0.5
Interfaces between *inboards* and *vlayers* with Ports[2]	0.5

according to *ANSYS*. The present model has a minimum and maximum skewness of 9.9461e-9 and 0.86723, respectively, and a minimum and maximum orthogonal quality of 0.24427 and 0.99999, respectively [46].

Table 3.3: Mesh skewness metrics spectrum

Excellent	**Very Good**	**Good**	**Acceptable**	**Bad**	**Unacceptable**
0 - 0.25	0.25 - 0.50	0.50 - 0.80	0.80 - 0.94	0.95 - 0.97	0.98 - 1.00

Table 3.4: Orthogonal quality mesh metrics spectrum

Unacceptable	**Bad**	**Acceptable**	**Good**	**Very Good**	**Excellent**
0 - 0.001	0.001 - 0.14	0.15 - 0.20	0.20 - 0.69	0.70 - 0.95	0.95 - 1.00

3.4 Problem Setup

Fluent 14.0 is the software used to perform the simulation; it has a very simple and direct setup tree which makes it very attractive for most users. The case setup is discussed at this point.

It is of good practice to check the mesh for any negative cell volumes, which is not the case. Due to the nature of the problem, transient is enabled for the time solver, the type of solver is pressure-based and the velocity formulation is kept as absolute. Double precision is enabled for more accurate results [47].

3.4.1 Models, Materials and Cell Zone Conditions

Fluent offers a great variety of models for the most diverse setups. For this setup, two models are used:

1. Energy Model - Activates the energy equation which is related to energy or/and heat transfer.

[1]Sweep Method is used.

[2]This meshing is used in order to match both meshing zones at each interface.

2. Viscous Model - The viscous model enables the study of inviscid, laminar and turbulent flows. Here, the Standard $\kappa-\varepsilon$ model is chosen, with *Standard Wall Treatment* activated. All model constants are maintained as default.

The material used is air with the *ideal-gas law* and *piecewise-polynomial* enabled for density and heat constant, respectively. The settings for the heat constant are maintained as default.

The operating pressure is defined as atmospheric (101325 Pa).

3.4.2 Boundary Conditions

Four types of boundary conditions are used in this model: *wall*, *interface*, *pressure-inlet* and *pressure-outlet*. The *wall* condition is applied to all cylinder and chamber walls, as well as the piston faces, valves and port walls. All cylinder walls, as well as valve and port walls have a constant temperature of 373.15 K. The *interface* boundaries are applied to those where two faces of different zones are in contact. The *pressure-inlet* is applied to the intake and *pressure-outlet* to the exhaust faces (see Tab. 3.5 and 3.6, respectively). *Pressure-inlet* is adequate when the intake pressure is known, but flow rate and/or velocity is not. Also, it is suitable for both compressible and incompressible flows. The *pressure-outlet* normally presents better rate of convergence results when *backflow* occurs than the *outflow* boundary condition.

Table 3.5: Inlet boundary conditon parameters

Pressure Inlet		
Momentum	Reference Frame	Absolute
	Gauge Total Pressure	0 Pa (Constant)
	Supersonic/Initial Gauge Pressure	0 Pa (Constant)
	Direction Specification Method	Normal to Boundary
	Specification Method	Intensity and Hydraulic Diameter
	Turbulent Intensity	2%
	Hydraulic Diameter	55.25 mm
Thermal	Total Temperature	323.15 K (Constant)

Table 3.6: Outlet boundary conditon parameters

Pressure Outlet		
Momentum	Gauge Pressure	0 Pa (Constant)
	Backflow Direction Specification Method	Normal to Boundary
	Specification Method	Intensity and Hydraulic Diameter
	Backflow Turbulent Intensity	2%
	Backflow Hydraulic Diameter	59 mm
Thermal	Total Temperature	323.15 K (Constant)

3.4.3 Dynamic Mesh

Normally, as most of numerical simulations are steady, dynamic meshing is not required; however due to the existence of moving parts in the geometry, which will deform the mesh, this feature is necessary. Meshing methods, in-cylinder parameters, events and moving bodies are defined in this section.

All three available meshing methods are enabled. *Smoothing* and *remeshing* options are available only for unstructured meshes, while *layering* performs on structured meshes. *Smoothing* enables the tetrahedra to act with a spring behavior allowing it to deform as smooth as possible. As the cells are deformed, they may reach a point where some present high skewness or very low quality, which is undesirable since it greatly affects the results obtained. When this occurs, *remeshing* is activated and performs several operations, based on user pre-defined conditions, which remeshes the affected zone in order to limit the cell values to the imposed conditions. The only zone in the model that requires these meshing methods is the chamber due to the valve motion. On the other hand, *layering* behaves similarly as the smoothing method; however, it only performs on structured meshes. By imposing a split factor (for when the cell height is increasing) and a collapse factor (for when the cell height is decreasing) it is possible to control cell quality and avoid negative cell volumes. Tab. 3.7 presents the parameters used for all mesh methods.

Table 3.7: Mesh method parameters

Mesh Methods		
Smoothing	Method	Spring/Laplace/Boundary Layer
	Spring Constant Factor	1
	Boundary Node Relaxation	1
	Convergence Tolerance	0.001
	Number of Iterations	20
Layering	Options	Ratio Based
	Split Factor	0.4
	Collapse Factor	0.05
Remeshing	Remeshing Methods	Local Cell & Region Face
	Minimum Length Scale	0.1 mm
	Maximum Length Scale	1.5 mm
	Maximum Cell Skewness	0.9
	Size Remeshing Interval	1

The *In-cylinder* option is also enabled, allowing the user to define cylinder parameters, such as engine speed, crank radius and minimum valve lift (Tab. 3.8). The minimum valve lift parameter enables the user to define a value, at which the valve is closed. In other words, since the valve cannot be fully closed due to the degeneration of the cells between the valve and the valve seat, a minimum lift is imposed in order to define the closing position of the valve.

Table 3.8: *In-cylinder* parameters

Parameters	
Crankshaft Speed	2500 rpm
Starting Crank Angle	0°
Crank Period	600°
Crank Angle Step Size	0.25°
Crank Radius	80 mm
Connecting Rod Length	290 mm
Piston Pin Offset	0 mm
Piston Stroke Cutoff	0 mm
Minimum Valve Lift	0 mm

In transient flows, such as the case in study, the *events* option can be used to time certain events

during the course of the simulation. These events allow the user to create and delete sliding interfaces, activate and deactivate cell zones and change the time-step or the Under-Relaxation Factors (URF). The events used for this simulation are described in the App. E.2.

The reason why the URF's and time-steps are reduced before valve opening is due to the great changes existent in the flow during this period. Also, when the valves are closed the zones above them (port area and *vlayer*) do not influence the cylinder flow, thus these can be deactivated. Consequently, the number of cells calculated during the closed valve period is greatly reduced.

Finally, the *dynamic mesh zones* are defined as *stationary*, *rigid body* or *deforming*. *Stationary zones*, as the word suggests, are the boundaries or zones that do not move. Normally, these are only defined when the adjacent zones are moving. *Rigid bodies* are those that have a rigid body behavior, without deforming its mesh. The *deforming zones* define the zones that are subjected to mesh deformations. The dynamic zones are explained in the App. E.4 and the valve profile is displayed in App. F

3.5 Solution

The solution section introduces the main tasks in solving any CFD simulation, such as defining spatial discretization schemes, solution limits, solution initialization, solution convergence and starting the simulation.

Solution Method

Having a pressure-based solver, the pressure-velocity coupling scheme chosen is PISO, mainly due to its great performance in transient cases and maintaining a stable calculation. Both *skewness* and *neighbor correction* are defined as 1. *Skewness correction* significantly reduces convergences issues associated with highly distorted meshes and providing a solution of a highly skewed mesh with quite the same number of iterations required for an orthogonal mesh. In transient cases, the number of iteration for convergence can be drastically reduced by activating *neighbor correction*. To avoid conflict of objectives, the *skewness-neighbor coupling* is disabled since it may cause divergence of the solution or lack of robustness.

The gradient spatial discretization is the *Green-Gauss Node-Based* scheme. The node-based scheme is known to be more accurate than the cell-based and performing better on unstructured meshes, despite being more computational expensive. For the pressure spatial discretization, PRESTO! is highly recommended in situations with great pressure variations in strong swirling flows, such is the case. For the remaining variables, second-order upwind scheme is chosen, with the exception of the dissipation rate (ε). First-order upwind scheme may have better convergence, but it is prone to give less accurate results, when compared to the second-order upwind scheme.

Solution Controls

URF's controls the influence of the previous variable result on the new one, which reduces the change of the variable between iterations. Tab. 3.9 presents the URF values for each variable

and in App. E.3 the applied changes before valve opening are shown.

Table 3.9: Under-Relaxation Factors

URF	
Pressure	0.3
Density	1
Body Forces	1
Momentum	0.7
Turbulent Kinetic Energy	0.4
Turbulent Dissipation Rate	0.4
Turbulent Viscosity	1
Energy	1

Temperature limits are changed to a minimum of 300 K and a maximum of 1500 K; minimum and maximum pressure are also altered to 1000 Pa and 5e7 Pa, respectively.

Monitors

The residual monitor performs iterative convergence checking in order to verify if each equation is converging to a defined value. Even though convergence should not be seen as a unique factor of good results, it is important for the residual equations to round-off to a user-defined value (usually very small depending if the calculation is done resorting to single or double precision). *Absolute convergence* criterion is applied in this case and the default values set, with the exception of continuity where the value is set to 1e-3.

Surface monitors are used to study mass flow rate through each valve interface in order to have an estimate of what enters and what leaves the cylinder and chamber. Temperature, pressure and skewness within the cylinder and chamber are monitored by implementing *volume monitors*.

Solution Initialization

In order for the first iterations to converge rapidly, it is advised to give good initial values. All variables are assigned with 0, with the exceptions of temperature (323.15 K), turbulent kinetic energy and turbulent dissipation rate - 1 m^2/s^2 and 1 m^2/s^3, respectively. Afterwards, in-cylinder temperature and pressure are patched with 1081 K and 3000000 Pa, respectively. Pressure is estimated by Eq. 3.9 and rounded up to the final value. Multiplying by two is due to the existence of two pistons.

$$p = 2c_r \gamma p_{atm} \tag{3.9}$$

Calculation

The solution is run with a fixed time stepping method, a total of 2440 time steps, which corresponds to 600º, and a maximum of 40 iterations per time step.

Chapter 4

Results

Over the course of one year, numerous simulations were performed, which the majority was not concluded due to various obstacles and problems. Initially, as mentioned in Sec. 3.3.1, only half of the geometry was considered, due to its symmetry; however, during the simulation, the mesh on the symmetry face of the chamber and adjacent to the interface of the *vlayer*, would begin to stretch and would not perform *remeshing*, according to the defined parameters. After contacting the *ANSYS* Technical Support Team, it was told that the symmetry face was not being considered, by the software, to perform both *smoothing* and *remeshing* functions. Thus, it was advised to consider the geometry as a whole in order to be able to go through with the simulations. Even though the problem was solved, another one arose: the computational cost and, hence the time for each simulation, grew drastically.

By considering the whole domain, the number of cells increased in the order of 3000000 to 3700000 cells; however, until then, the range of the cell count was much less: 500000 to 1000000 cells. This increase of cells was due to two causes in particular. The first cause, as mentioned above, was the increase in the domain size. Divergence issues during the simulation, as well as low quality results, was cause number two; during the calculations, warnings would appear informing that the solution was diverging and would ultimately stop. This issue was solved by gradually decreasing the size of each mesh element in each necessary zone, until the solution divergence was avoided.

The increase of the number of cells also led to a greater computational cost; initially, each simulation would take a few days to be concluded (this is an estimation considering the time taken to calculate the number of time steps until stopping). Afterwards, each simulation took about three weeks and in some cases took more than a month. Of course all this depends on the type of machine available. For the current solution, a machine with an eight core processor and 30 GB of RAM was used.

The results presented in this chapter are considered to be the best among the simulations performed, even though they did not achieve the authors expectations or goals. 1856 time steps in 2440 scheduled were completed with a total of 38200 iterations, approximately; time and computational cost were the main issues during this simulation for not completing the total number of time steps. Several parameters were evaluated and analyzed throughout the simulation: static pressure and temperature, flow velocity and Mach number, mass flow rate in and out of the cylinder, fluid density and chamber cell skewness.

As expected, during the expansion stage (the initial 520 time steps) a decrease of both pressure and temperature is visible within the cylinder as presented in Fig. 4.1 and Fig. 4.2, respectively. During this period no fluid left or entered the cylinder through each valve, as seen in Fig. 4.3 and Fig. 4.4.

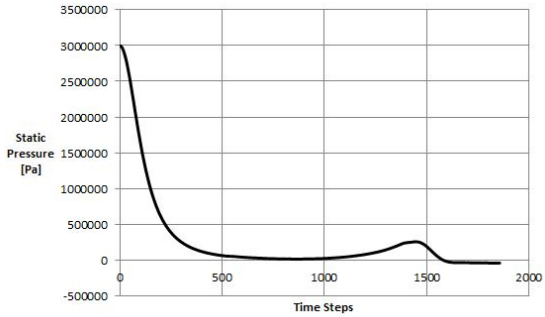

Figure 4.1: In-cylinder static pressure

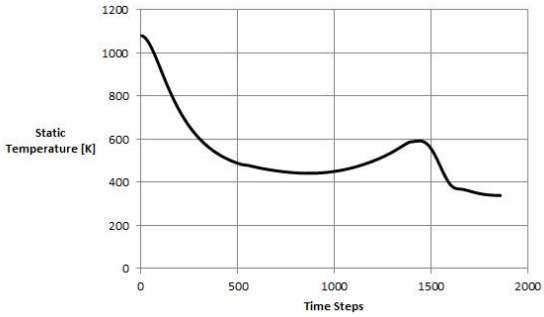

Figure 4.2: In-cylinder static temperature

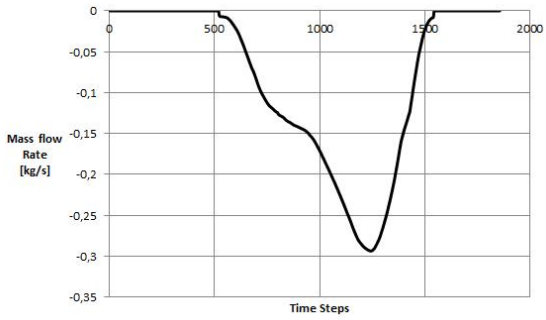

Figure 4.3: Mass flow rate through the exhaust valve

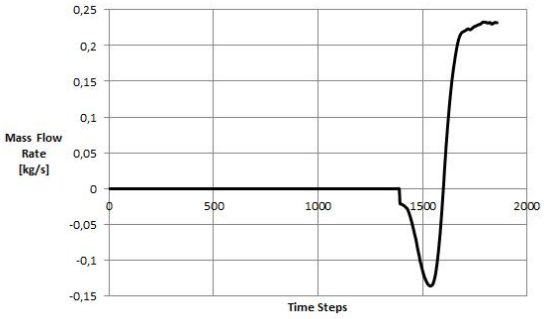

Figure 4.4: Mass flow rate through the admission valve

From a more visual perspective[1], Fig. 4.5 shows that the fluid is "drawn" out of the chamber into the cylinder zone; by the time the exhaust valve opens, in-cylinder temperature was reduced by a factor of two and static pressure was about half of atmospheric pressure (Fig. 4.6 and Fig. 4.7, respectively). The absolute pressure in the cylinder was still greater than the exhaust port which led to a slightly visible *blowdown* during the initial phase of the exhaust process (see Fig. 4.3).

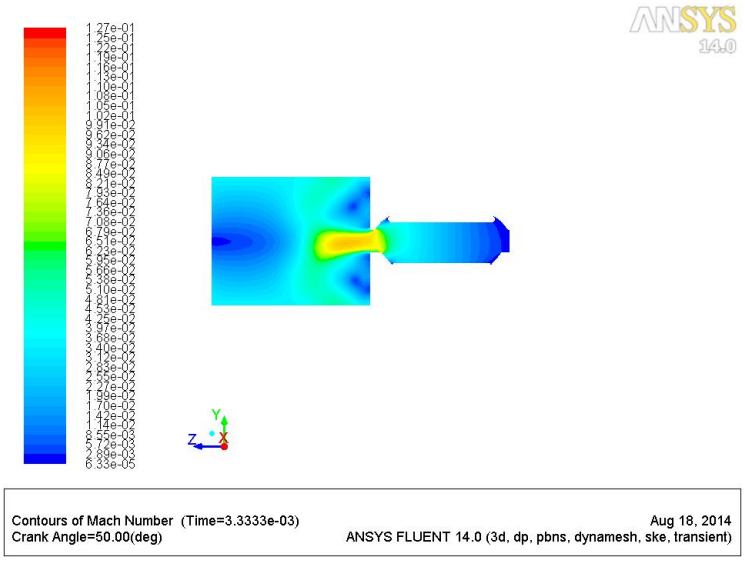

Figure 4.5: Contours of Mach number at 50° crank angle

[1] All the contours are presented in their symmetrical view.

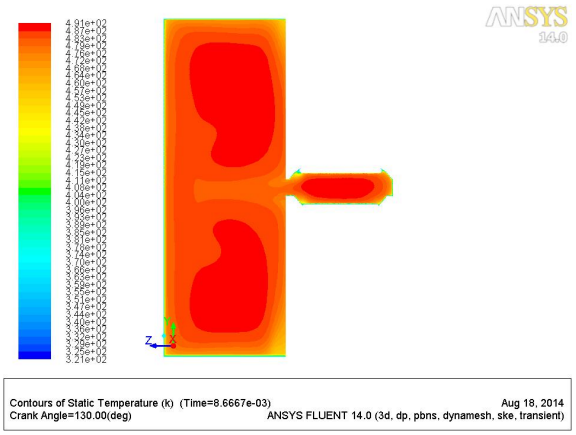

Figure 4.6: Contours of static temperature at 130° crank angle (before exhaust valve opening)

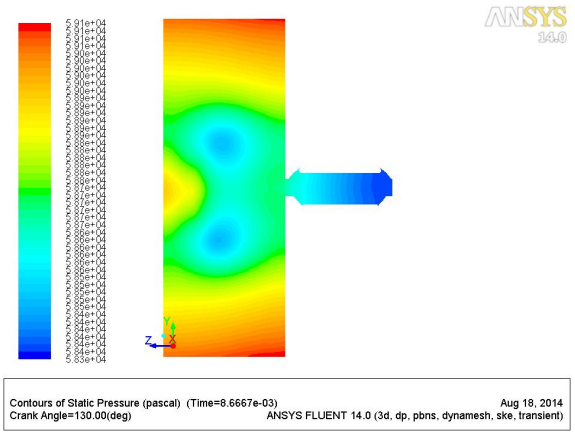

Figure 4.7: Contours of static pressure at 130° crank angle (before exhaust valve opening)

As the exhaust valve continues to open, the velocity in the gap near the valve head increases rapidly due to the very tight opening (Fig. 4.8) and then slowly decreases until 190°. After this point, the flow separates at the rear end of the valve (Fig. 4.9) and the Mach number gradually begins to increase, reaching a maximum of Mach 2.2 at TDC position. It is believed that these abnormal values appear mainly due to the geometry of the cylinder/chamber; as both pistons move towards the TDC, fluid is pushed through the narrow opening into the chamber and flows directly through the front and lateral sides of the valve gap, meaning that nearly half the valve is not used properly. Also, flow at the exhaust port has been influenced by its behavior when exiting the cylinder, thus the direct effect of the exhaust port on the flow is unknown (see Fig. 4.10).

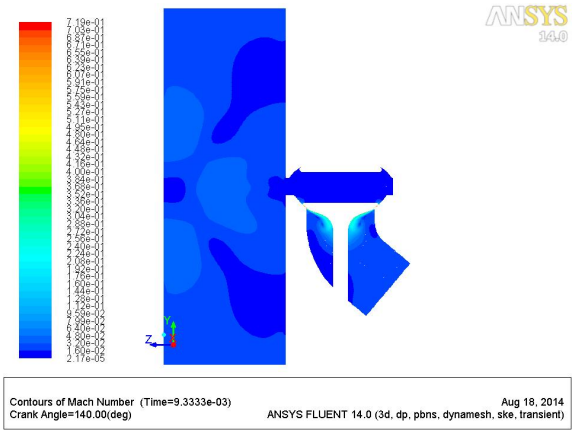

Figure 4.8: Contours of Mach number at 140° crank angle

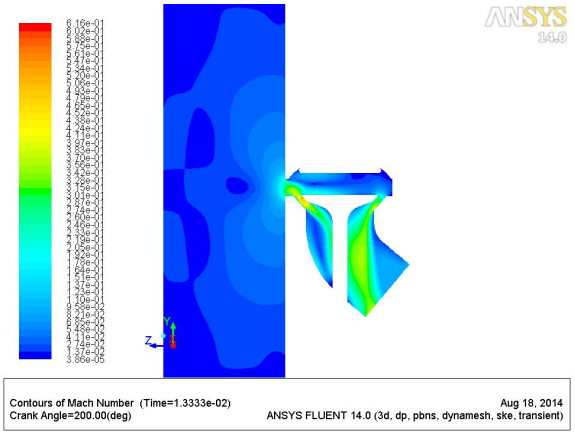

Figure 4.9: Contours of Mach number at 200° crank angle

The fact that the valve is not functioning properly may explain the abnormal rise in both pressure and temperature midway the exhaust stroke. Again, it is not clear if the issue is the valve design and dimensioning or the geometry of the cylinder/chamber. Nevertheless, the extremely high speeds at the valve throat, besides being completely destructive, chokes the flow and drastically reduces the mass flow rate.

Slightly after the admission valve opens, both pressure and temperature decrease again, since

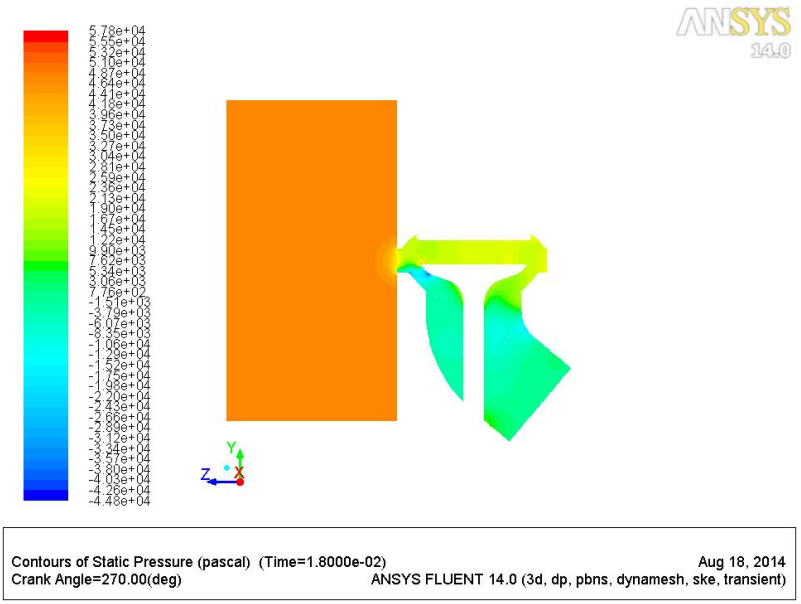

Figure 4.10: Contours of static pressure at 270º crank angle

in-cylinder pressure is greater than the admission port and so the flow exits the cylinder through the admission valve. It is known that this occurrence is usual, however it is not desirable, especially when it occurs for long periods of time. Only when the in-cylinder pressure decreases to values near or lower than the admission port does the flow enter the cylinder (see Fig. 4.11). Similarly to what happens at the exhaust valve, only one side of the admission valve functions properly; due to the suction created the fluid also enters the cylinder directly from one side of the valve leading to a poor performance of the other remaining half. Fig. 4.11 shows precisely that near the valve throat.

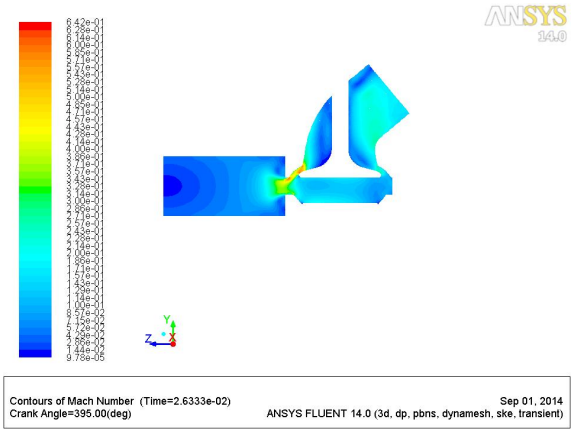

Figure 4.11: Contours of Mach number at 395º crank angle

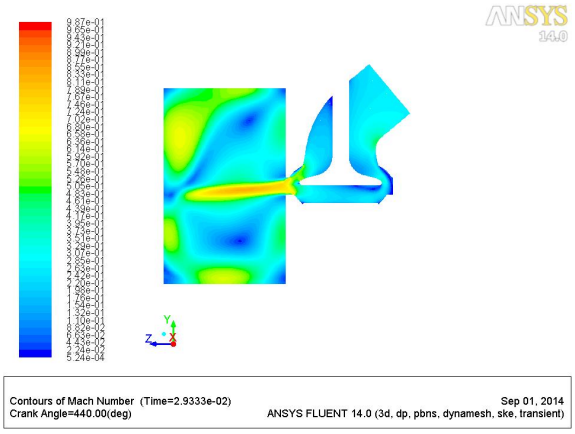

Figure 4.12: Contours of Mach number at 440º crank angle

It is visible in Fig. 4.12 the high value of Mach number, not at the valve throat, but at the passage from the chamber to the cylinder. As both pistons move towards their BDC, a suction effect is created in the cylinder and withdraws fluid from the chamber and the admission port. Possibly, due to poor mass inflow rate, pressure in the cylinder begins to decrease greatly when compared to the chamber (see Fig. 4.13) and, as a consequence, velocity increases. However, for the Mach number to increase, the speed of sound and temperature must decrease, since the Mach number is indirectly proportional to temperature (Eq. 4.2). Eq. 4.2 is derived from the

Eq. 2.27 and Eq. 4.1, the latter being the ideal-gas equation. The density of the fluid slightly decreases in the passage region (Fig. 4.14) (considering that the density is greater in the chamber and less in the cylinder), however the velocity of the fluid is still much greater (Fig. 4.15) and overcomes the influence of density, resulting in a decrease of temperature (Fig. 4.16). Due to this variation of temperature, limiters were activated during the simulation in order to impose a temperature of 300 K or otherwise the temperature would continue to decrease until reaching impossible values for IC engines, such as 250 K or less.

$$p = \rho RT \tag{4.1}$$

$$M^2 = \frac{U^2 \rho}{p\gamma} \tag{4.2}$$

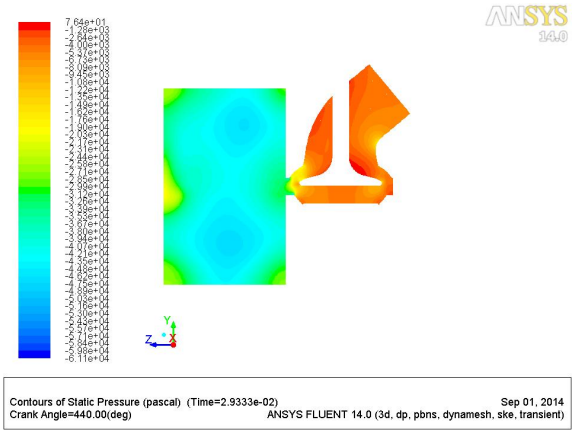

Figure 4.13: Contours of pressure at 440º crank angle

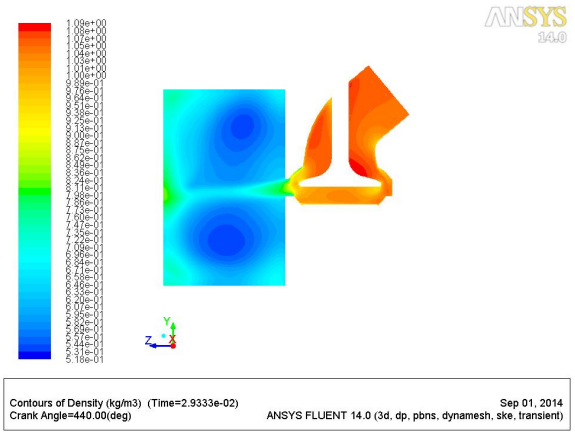

Figure 4.14: Contours of density at 440º crank angle

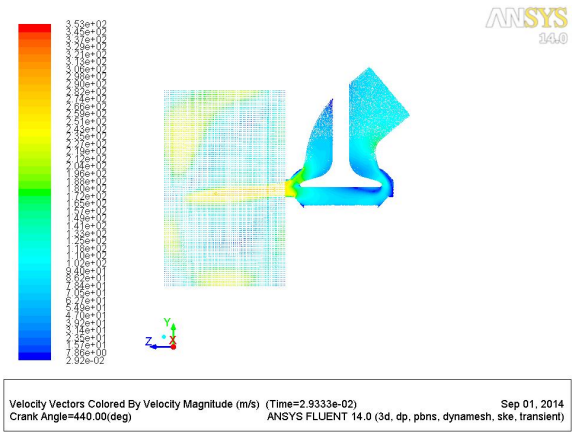

Figure 4.15: Velocity vectors at 440º crank angle

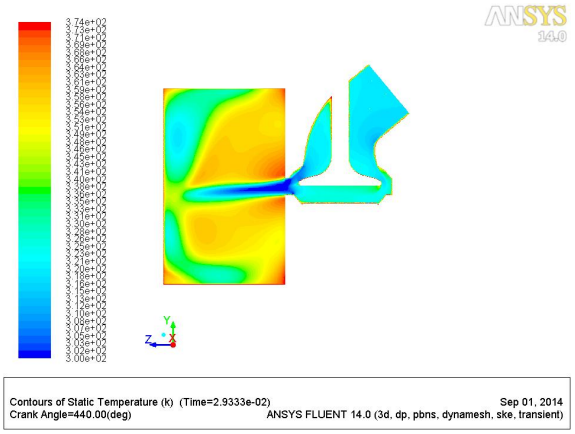

Figure 4.16: Contours of static temperature at 440º crank angle

Hence that, as the valve head diameter increases so does the chamber volume , which leads to the necessary decrease of the clearance height (distance between both piston heads), due to the predefined compression ratio as well as the limited space for the valves to move. This can bring very narrow passages and, consequently, undesired flow velocities. With a 15 mm height

at this passage, it is possible that it may have a strong influence on the flow behavior. All these factors combined resulted in a poor in-cylinder flow and influenced the outcome of the total cycle.

Chapter 5

Conclusions

This study presents a numerical analysis of a four-stroke OP engine with the use of CFD tools, in this case *ANSYS Fluent 14.0*. Both chamber and valves were dimensioned by the author, as well as its design in *CATIA V5* and CFD modeling. The purpose of this study was to analyze overall in-cylinder and port flow properties in order to verify the viability of a four-stroke cycle for this type of engine. Challenges are always expected in a study of this nature, especially when it comes to model dimensioning; the present chapter explains the possible problems and solutions in order to improve the results, as well as the results obtained and future studies.

The concept itself is challenging, mostly due to the lack of space for conditioning both valves, but also for dimensioning reasons. With the increase of valve head diameters, the clearance volume will also increase leading to very low compression ratios; this is far from today's requirements and the solution for maintaining the compression ratio at a desired level is to lower the height between both piston heads. This solution also brings other problems regarding valve lift and flow properties. It was seen in Sec. 4 that having a very narrow passage between the chamber and cylinder, led to significant incompatible results regarding IC engines. The chamber design, as well as both piston heads, can and should be redesigned in order to improve in-cylinder flow.

By mentioning redesigning both chamber and pistons, it is also of the authors understanding that both valves and respective ports need a review on its design and its location. The fact that each valve has only one side facing the cylinder zone, leads to inefficient exhaust and admission phases. Initially, when the pressure is sufficiently greater or less in the cylinder, the fluid that exits or enters through the valve gap, does so in a very uniform way: the entire gap functions as it is supposed to. However, as valve lift increases and pressure difference becomes greater, the fluid begins to be "sucked" out of the valve laterally. The valve becomes inefficient, since only half of the valve is actually allowing fluid to exit or enter the cylinder. A possible solution was encountered: the creation of an "air socket" or a kind of perforation in the chamber and place each valve within this socket. This idea would allow the valve to have an equivalent pressure surrounding the valve gap, as well as avoid the direct suction effect from one side of the valve. However, this idea would lead to a very large clearance volume, especially when very large valves are present.

Decomposition showed to be a very good solution when dealing with moving parts. By creating geometries that allow the use of structured meshing, such as the *inboard* and *vlayer*, the time and computational cost was reduced greatly. The mesh generation, although the number of cells was extremely high, was appropriate for the case, having decent orthogonal quality and skewness. Nevertheless, improving skewness quality would directly affect the solution for the best. Regarding dynamic meshing, the solution behaved as expected with all events occurring at the defined time, as well as all three meshing methods performed as predicted.

As for the results obtained from the CFD analysis, these can be brought down to three stages: expansion, exhaust and admission stages. The expansion stage performed as expected, with both pressure and temperature decreasing. When the exhaust valve opens, initially, fluid is pushed out through the whole surrounding of the valve; however, as this stage continues, Mach number at the valve throat reaches unbearable values, as well as the in-cylinder pressure and temperature increase due to the inability of the valve to expel the gases. Finally, the admission stage, similarly to the previous one, performs well at the beginning, but the duration of reverse flow from the cylinder to the admission port is far too long. Plus, the valve cannot deliver the amount of air necessary at the needed rate and, at the passage from chamber to cylinder, velocity reaches once again very high values.

Unfortunately, the simulation did not reach the 2440 time step goal, however with the available results, it was possible to evaluate and predict the final outcome of the solution. It is the author's opinion that adapting an OP engine to function at a four-stroke cycle still cannot be dismissed, however the engine of reference for this case is to large in order to function as so, since neither the exhaust and admission processes produced the expected results. Possibly, OP engines with a smaller bore and/or stroke can be used to be adapted as a four-stroke.

5.1 Future Studies

As mentioned several times throughout this work, the variables involved in final engine parameters are extensive. This study was done based on certain parameters and variables, and left a countless number of situations yet to explore. In the future, more studies as such can be done which involve different engine parameters:

- Engine speed, stroke, bore, compression ratio - all these variables can be changed and studied;
- The engine geometry design has clearly showed that its influence should not be underrated;
- Number of valves, as well as their positioning, location and design are possibly the most difficult challenge;
- Valve timing and profile also have an influence on flow behavior;
- Port design should be adapted, in order to receive and give gases the best possible way.

These examples were mentioned, however much more are to be taken in account for, regarding the solution setup and mesh generation. The decomposition process is becoming everyday much easier and so are meshing and solution setup. The downfall regarding IC engine CFD analysis is time and computational cost. If the available machines are not suitable for the case, the waiting process can be very painful. Nevertheless, the price to pay is much less than if a prototype was to be built.

Bibliography

[1] D. Johnson, M. Wahl, F. Redon, E. Dion, S. McIntyre, G. Regner, and R. Herold, ``Opposed-piston two-stroke diesel engine-a renaissance," in *Symposium on International Automotive Technology (SIAT)*, 2011. 1

[2] R. D. Reitz, ``Directions in internal combustion engine research," *Combustion and Flame*, vol. 160, no. 1, pp. 1 -- 8, 2013. 2

[3] J. Pirault and M. Flint, *Opposed Piston Engines: Evolution, Use, and Future Applications*. SAE International, 2010. 3, 6

[4] W. Hees, ``Improvement in gas-engines," Mar. 25 1879, uS Patent 213,539. 4

[5] G. SureshBabu, S. Jagadeesh, U. Saicharan, and P. Praneeth, ``Analysis of a single cylinder combustion engine using cfd," *International Journal of Innovative Technology and Exploring Engineering*, vol. 4, no. 5, 2013. 4

[6] (2008) Der werftverein. [Online]. Available: http://www.der-werftverein.de/akr/jumo205c/jumo205_getriebe.html 6

[7] M. Nabavi and K. Siddiqui, ``A critical review on advanced velocity measurement techniques in pulsating flows," *Measurement Science and Technology*, vol. 21, no. 4, p. 042002, 2010. 8

[8] J. D. Denton, ``Some limitations of turbomachinery cfd," in *ASME Turbo Expo 2010: Power for Land, Sea, and Air*. American Society of Mechanical Engineers, 2010, pp. 735--745. 8

[9] F. Brójo, A. Santos, and J. Gregório, ``Computational analysis of the scavenging of a twostroke opposed piston diesel engine," in *The 2010 International Conference of Mechanical Engineering, London, UK*, vol. 30, 2010. 8

[10] Z. Zhang, C. Zhao, F. Zhang, and F. Guo, ``Modeling and simulation of dq opposed-piston two-stroke diesel engine," *Stroke*, vol. 2000, p. 110, 2012. 9

[11] A. Lakshman, C. Karthikeyan, and R. Padmanabhan, ``3d in-cylinder cold flow simulation studies in an ic engine using cfd." 9

[12] N. Semin, R. A. B. Ibrahim, and R. I. Abdul, ``In-cylinder flow through piston-port engines modeling using dynamic mesh," *Journal of Applied Sciences Research*, vol. 4, no. 1, pp. 58--64, 2008. 9

[13] S. R. Pitta and R. Kuderu, ``A computational fluid dynamics analysis on stratified scavenging system of medium capacity two-stroke internal combustion engines," *Thermal Science*, vol. 12, no. 1, pp. 33--42, 2008. 10

[14] M.-j. Luo, G.-h. Chen, and Y.-h. Ma, ``Three-dimensional transient numerical simulation for intake process in the engine intake port-valve-cylinder system," *Journal of Zhejiang University SCIENCE A*, vol. 4, no. 3, pp. 309--316, 2003. 10

[15] E. Pariotis, G. Kosmadakis, and C. Rakopoulos, ``Comparative analysis of three simulation models applied on a motored internal combustion engine," *Energy Conversion and Management*, vol. 60, pp. 45--55, 2012. 10

[16] H. Jasak, J. Luo, B. Kaluderčić, A. Gosman, H. Echtle, Z. Liang, F. Wirbeleit, M. Wierse, S. Rips, A. Werner *et al.*, ``Rapid cfd simulation of internal combustion engines," SAE Technical Paper, Tech. Rep., 1999. 11

[17] (2010) Thermopedia. [Online]. Available: http://www.thermopedia.com/content/880/ 14

[18] R. A. Bakar and S. Semin, ``The internal combustion engine diversification technology and fuel research for the future: A review." 14

[19] R. Singal and M. Singal, *Engineering Thermodynamics*. I.K. International Publishing House Pvt. Limited, 2009. 15

[20] W. Pulkrabek, *Engineering Fundamentals of the Internal Combustion Engine*. Pearson Prentice Hall, 2004. 16

[21] G. D. Nicolao, R. Scattolini, and C. Siviero, ``Modelling the volumetric efficiency of ic engines: Parametric, non-parametric and neural techniques," *Control Engineering Practice*, vol. 4, no. 10, pp. 1405 -- 1415, 1996. 18

[22] R. B. Pešić, A. L. Davinić, S. D. Petković, D. S. Taranović, and D. M. Miloradović, ``Aspects of volumetric efficiency measurement for reciprocating engines," *Thermal Science*, vol. 17, no. 1, 2013. 18

[23] V. de Brederode, *Fundamentos de aerodinamica incompressível*. Lisboa: Edicao do autor, 1997. 19

[24] R. Huang, C. Huang, S. Chang, H. Yang, T. Lin, and W. Hsu, ``Topological flow evolutions in cylinder of a motored engine during intake and compression strokes," *Journal of Fluids and Structures*, vol. 20, no. 1, pp. 105 -- 127, 2005. 20

[25] J. Heywood, *Internal Combustion Engine Fundamentals*, ser. McGraw-Hill series in mechanical engineering. McGraw-Hill, 1988. 20, 21

[26] R. Stone, *Introduction to Internal Combustion Engines*. Society of Automotive Engineers, 1999. 21

[27] W. Annand and G. Roe, *Gas Flow in the Internal Combustion Engine: Power, Performance, Emission Control, and Silencing*. G. T. Foulis, 1974. 23

[28] S. Thirumalini, C. Lakshmikanthan, and S. Dhandapani, ``Cfd modelling for parametric investigation of flow through the inlet valve of a four-stroke engine." *International Journal of Applied Engineering Research*, vol. 4, no. 7, 2009. 23

[29] H. T. Toh, R. F. Huang, K. H. Lin, and M.-J. Chern, ``Computational study on the effect of inlet port configuration on in-cylinder flow of a motored four-valve internal combustion engine," *Journal of Energy Engineering*, vol. 137, no. 4, pp. 198--206, 2011. 23

[30] J. Blazek, *Computational Fluid Dynamics: Principles and Applications*. Elsevier Science, 2005. 27

[31] J. D. Anderson *et al.*, *Computational fluid dynamics*. Springer, 1995, vol. 206. 27

[32] C. Hirsch, *Numerical Computation of Internal and External Flows: The Fundamentals of Computational Fluid Dynamics: The Fundamentals of Computational Fluid Dynamics*. Elsevier Science, 2007, no. vol. 1. 28

[33] J. Tu, G. Yeoh, and C. Liu, *Computational Fluid Dynamics: A Practical Approach*. Elsevier Science, 2007. 29

[34] I. Celik, I. Yavuz, A. Smirnov, J. Smith, E. Amin, and A. Gel, ``Prediction of in-cylinder turbulence for ic engines," *Combustion science and technology*, vol. 153, no. 1, pp. 339--368, 2000. 31

[35] G. Thomas, M. University of Wollongong. School of Mechanical, and M. Engineering, *CFD Modelling and Analysis of an Opposed Piston Internal Combustion Engine*. University of Wollongong, 2009. 32

[36] ANSYS, ``Introduction to ansys fluent," 2010. 32

[37] *ANSYS Help*, ANSYS Inc. 32

[38] J. Boehning, ``Flathead adaption system for engine," May 17 1994, uS Patent 5,311,847. 33

[39] M. Clements, ``Cylinder head and valve configuration," Dec. 11 2001, uS Patent 6,328,012. 33

[40] G. Blair, ``Side valve arrangement for an internal combustion engine," Nov. 4 2003, uS Patent 6,640,780. 33

[41] T. Ebihara, H. Urata, and Y. Yamada, ``Side-valve type internal combustion engine," Sep. 26 1995, uS Patent 5,452,702. 33

[42] S. McKelvie. (2012) A critique of the "flathead" or side-valve-engine-design. [Online]. Available: http://stevemckelvie.wordpress.com/2012/07/12/a-critique-of-the-flathead-or-side-valve-engine-design/ 33

[43] R. Huang, H. Yang, and C.-N. Yeh, ``In-cylinder flows of a motored four-stroke engine with flat-crown and slightly concave-crown pistons," *Experimental Thermal and Fluid Science*, vol. 32, no. 5, pp. 1156 -- 1167, 2008. [Online]. Available: http://www.sciencedirect.com/science/article/pii/S0894177708000113 34

[44] ANSYS, ``Ic engine system," in *Automotive Simulation World Congress*, 2012. 34

[45] ``Setting up and solving a cold flow ic engine problem - tutorial," ANSYS. 35

[46] ``Introduction to ansys - meshing," ANSYS, 2012. 36

[47] ``Cold flow simulation inside an si engine - tutorial 12," ANSYS. 36

Appendix A

Jumo 205E

Table A.1: Jumo 205E data

Parameters	
Number of Cylinders	6
Bore	105 mm
Stroke	160 $mm \times 2$
Volume	16.6 L
Compression Ratio	17
Length	2.05 m
Height	1.32 m
Width	0.6 m
Weight	570 kg
Take-Off Power	552 kW
Cruise Power	417 kW
RPM	2500 rpm
Fuel Consumption	210.5 g/kWh
Break Thermal Efficiency	40.6 $\%$

Appendix B

Engine Model Details and Schematics

B.1 Detailed View of the Valve Gap

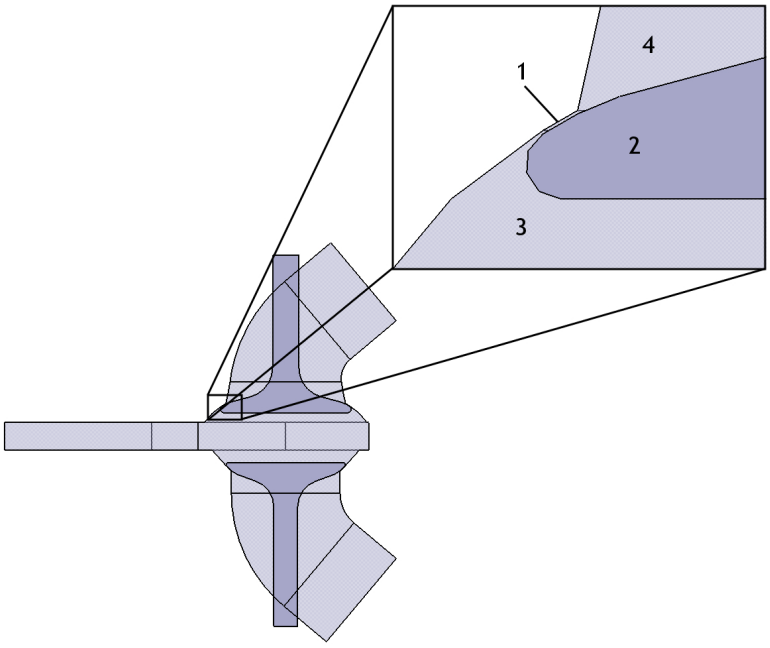

Figure B.1: Detailed view of the valve gap: 1 - Gap; 2 - Valve head; 3 - Combustion chamber; 4 - Port

B.2 Schematics of the Model Engine

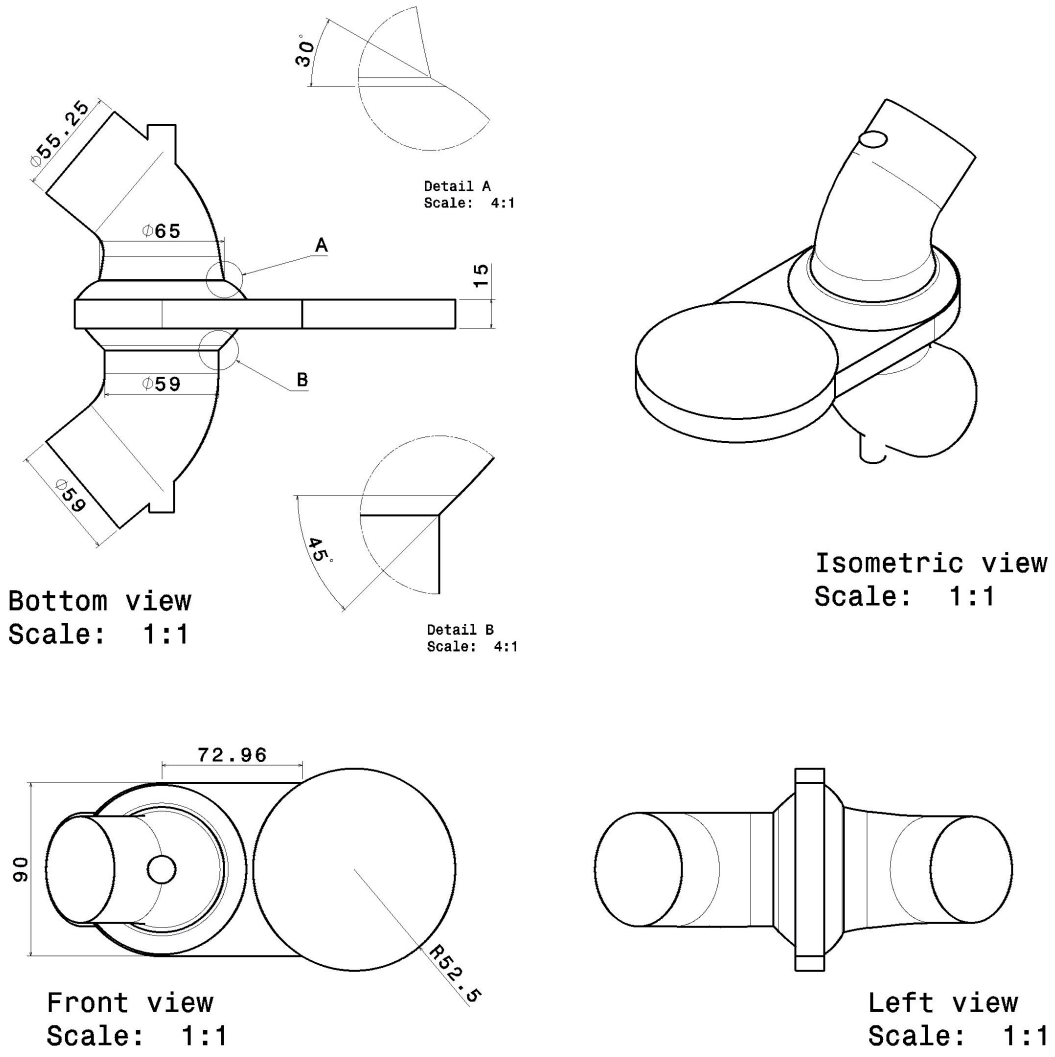

Figure B.2: Schematics of the model engine

Note: Units are in millimeters.

Appendix C

Geometry Decomposition and Boundary Naming

C.1 Geometry Decomposed

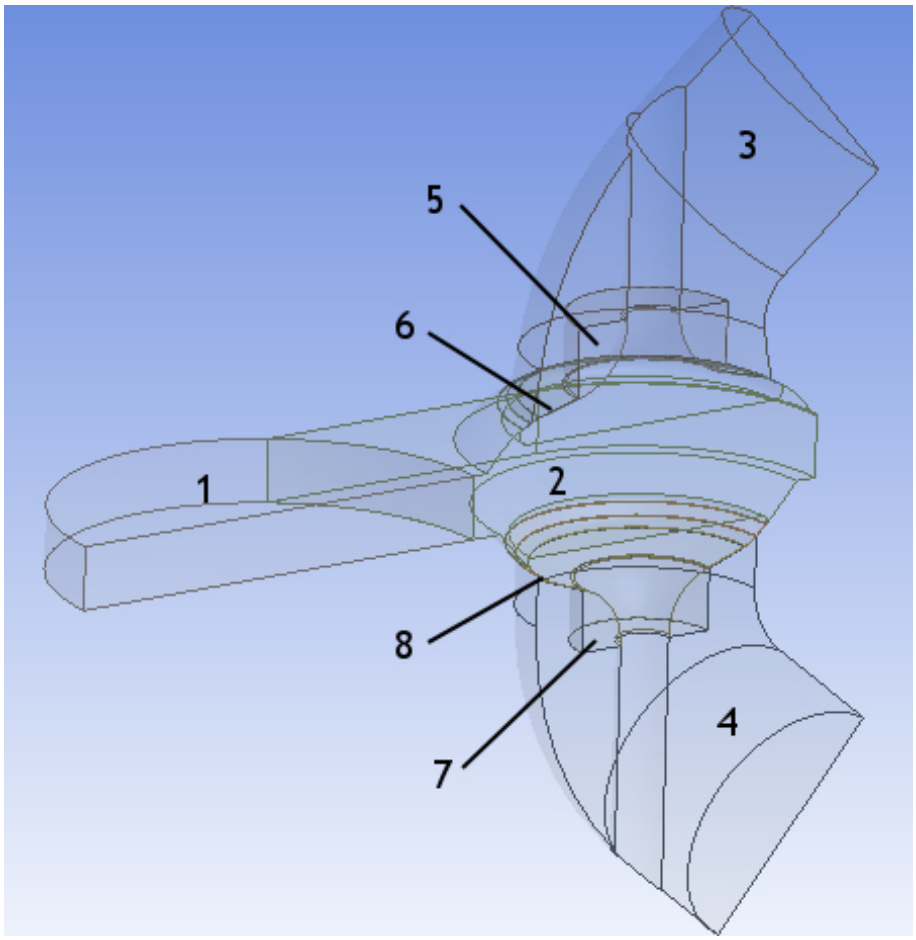

Figure C.1: Symmetrical view of the decomposed geometry

Table C.1: Geometry fluid domains

	Named Selections
1	fluid-cylinder
2	fluid-chamber
3	fluid-invalve-port
4	fluid-exvalve-port
5	fluid-invalve-inboard
6	fluid-invalve-vlayer
7	fluid-exvalve-inboard
8	fluid-exvalve-vlayer

C.2 Named Selections of both Cylinder and Chamber

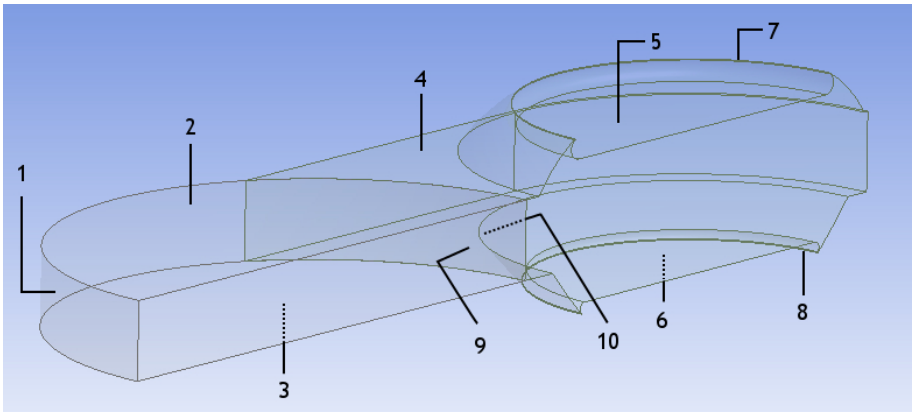

Figure C.2: Named selections of both cylinder and chamber

Table C.2: Cylinder and chamber boundary names

Named Selections Names	
1	cylinder-wall[1]
2	upper-piston[1]
3	lower-piston[1]
4	chamber-walls[1]
5	invalve-ch[1]
6	exvalve-ch[1]
7	intf-invalve-ob-fluid-ch[2]
8	intf-exvalve-ob-fluid-ch[2]
9	intf-cylinder[2]
10	intf-chamber[2]

[1]Wall
[2]Interface

C.3 Named Selections of both *Vlayers*

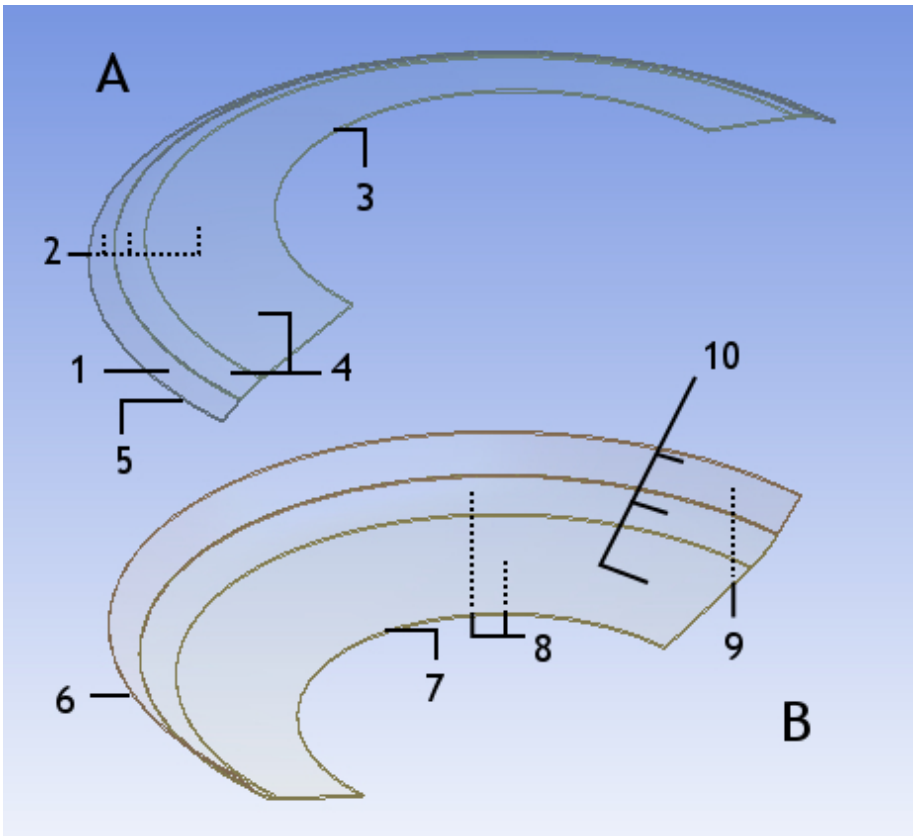

Figure C.3: Named selections of both *vlayers*: A - Invalve *vlayers*; B - Exvalve *vlayers*

Table C.3: Invalve and exvalve *vlayer* boundary name

	Named Selections Names
1	invalve-seat[1]
2	invalve-ob[1]
3	intf-invalve-ib-fluid-vlayer[2]
4	intf-int-invalve-ob-fluid-vlayer[2]
5	intf-invalve-ob-fluid-vlayer[2]
6	intf-exvalve-ob-fluid-vlayer[2]
7	intf-exvalve-ib-fluid-vlayer[2]
8	intf-int-exvalve-ob-fluid-vlayer[2]
9	exvalve-seat[1]
10	exvalve-ob[1]

[1]Wall
[2]Interface

C.4 Named Selections of both *Inboards*

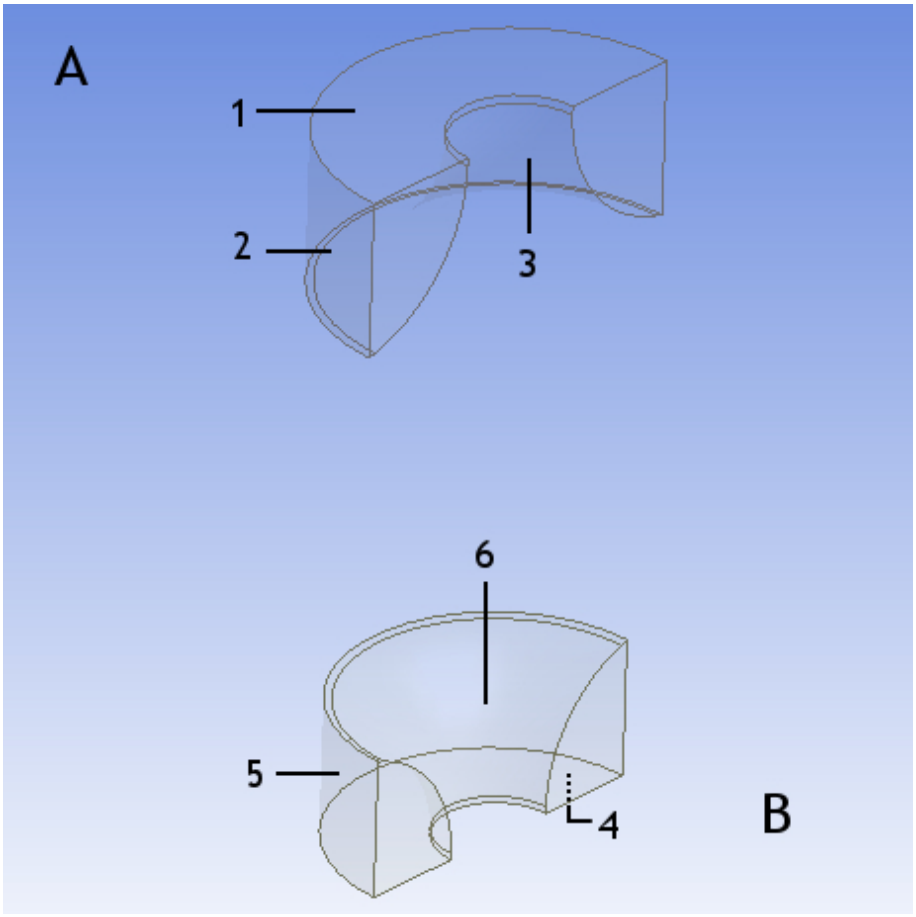

Figure C.4: Named selections of both *inboards*: A - Invalve *inboard*; B - Exvalve *inboard*

Table C.4: Invalve and exvalve *inboard* boundary names

	Named Selections Names
1	intf-int-invalve-ib-fluid-ib[2]
2	intf-invalve-ib-fluid-ib[2]
3	invalve-ib[1]
4	intf-int-exvalve-ib-fluid-ib[2]
5	intf-exvalve-ib-fluid-ib[2]
6	exvalve-ib[1]

[1]Wall
[2]Interface

C.5 Named Selections of the Admission Port

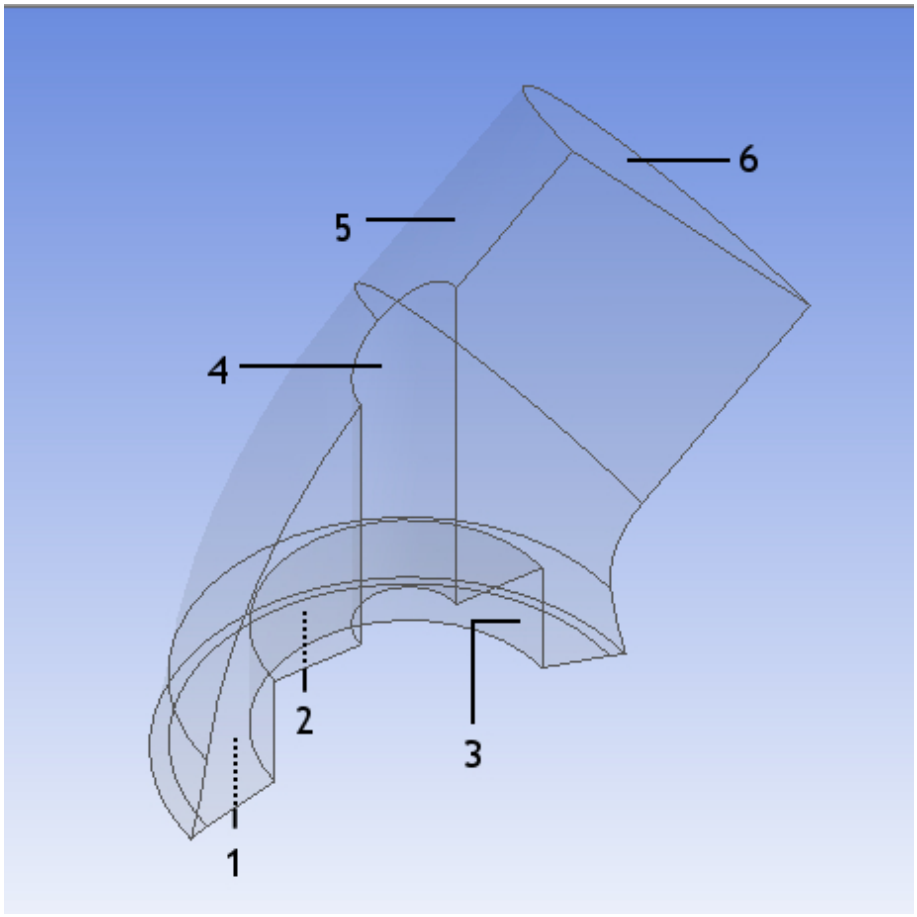

Figure C.5: Named selections of the admission port

Table C.5: Admission port boundary names

	Named Selections Names
1	intf-int-invalve-ob-fluid-port[2]
2	intf-int-invalve-ib-fluid-port[2]
3	intf-invalve-ib-fluid-port[1]
4	invalve-stem[1]
5	invalve-port-wall[1]
6	inlet[3]

[1]Wall
[2]Interface
[3]Pressure-inlet

C.6 Named Selections of the Exhaust Port

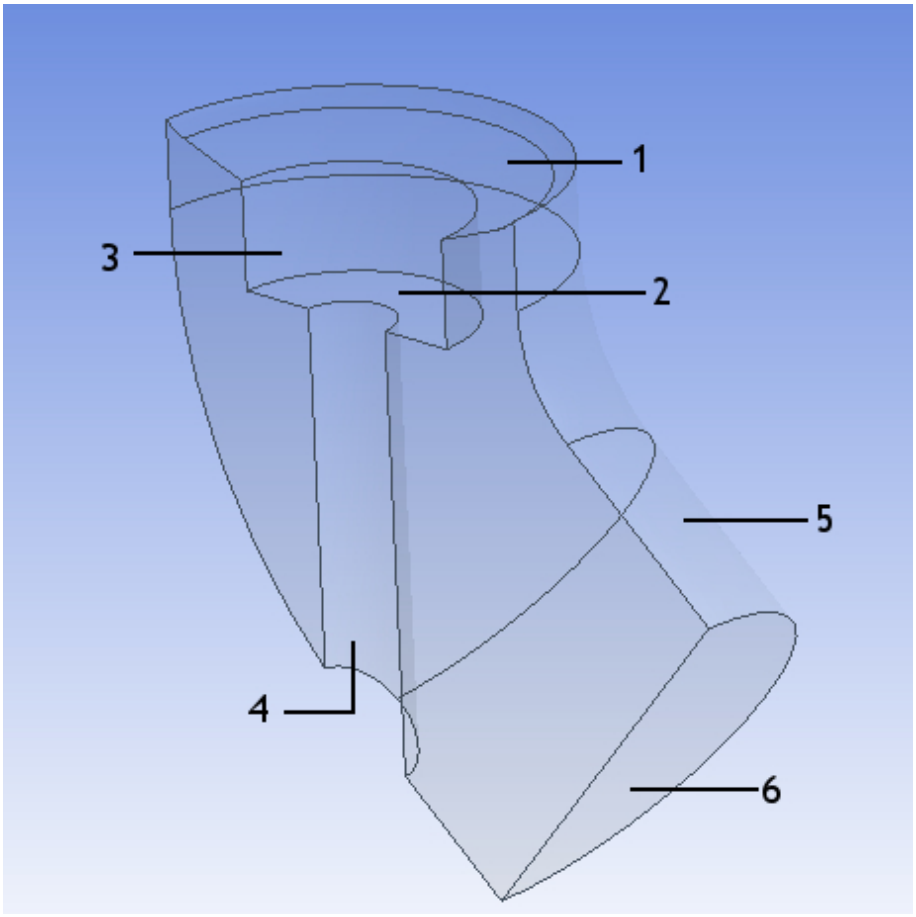

Figure C.6: Named selections of the exhaust port

Table C.6: Exhaust port boundary names

	Named Selections Names
1	intf-int-exvalve-ob-fluid-port[2]
2	intf-int-exvalve-ib-fluid-port[2]
3	intf-exvalve-ib-fluid-port[1]
4	exvalve-stem[1]
5	exvalve-port-wall[1]
6	outlet[3]

[1]Wall
[2]Interface
[3]Pressure-outlet

Appendix D

Mesh

D.1 Cylinder Mesh

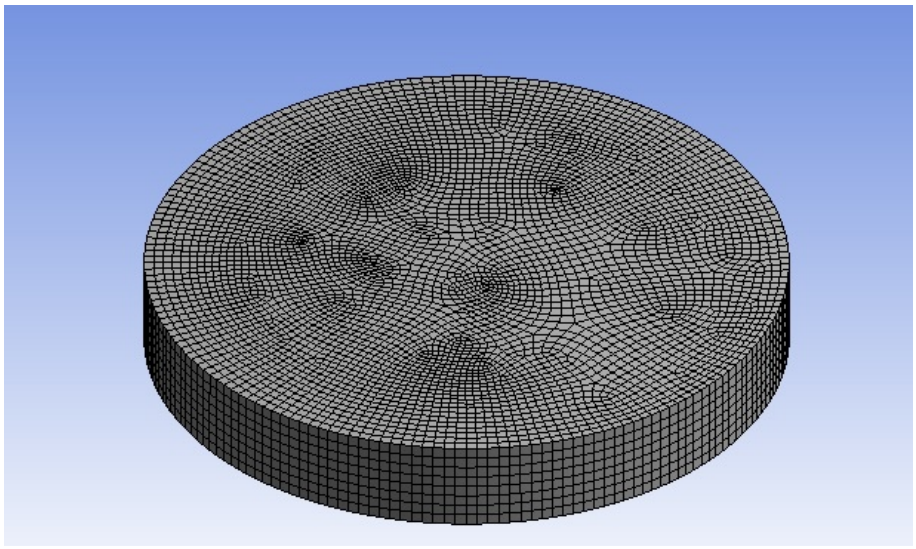

Figure D.1: Quadrilateral meshing in the cylinder domain

D.2 Chamber Mesh

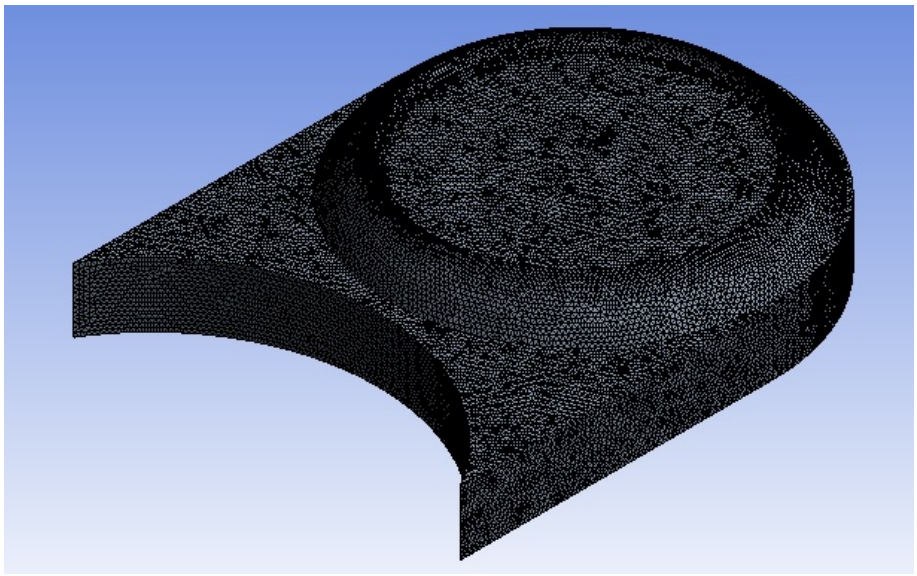

Figure D.2: Tetrahedral meshing in the chamber domain

D.3 Port Mesh

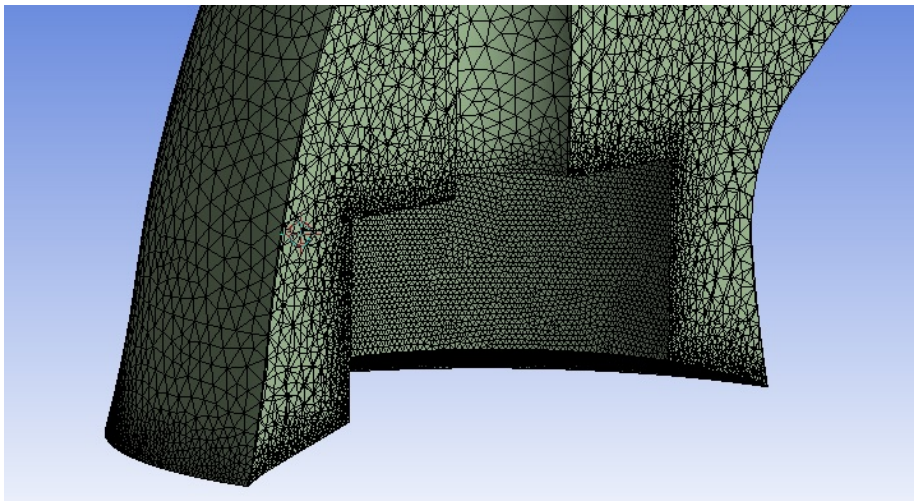

Figure D.3: Tetrahedral meshing in the admission port (similar to the exhaust port)

D.4 *Inboard* and *Vlayer* Mesh

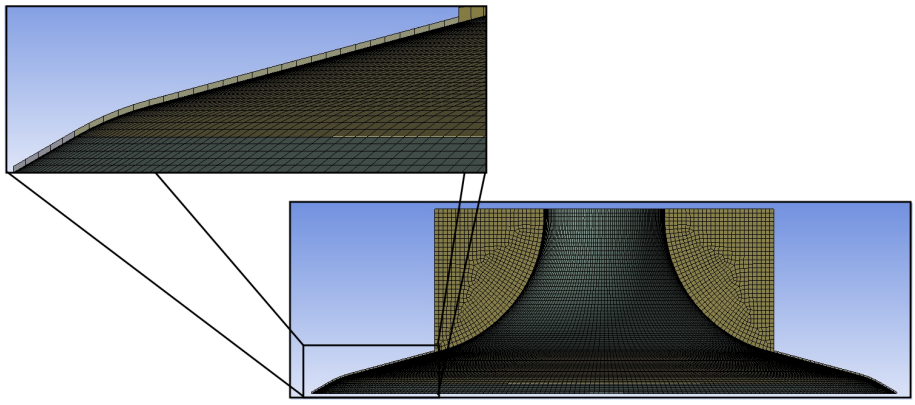

Figure D.4: One layer of quadrilateral meshing in the *vlayer* and a mixture of a greater number of quadrilateral with tetrahedral cells in the *inboard* (similiar to the exhaust *vlayer* and *inboard*)

Appendix E

Mesh Interfaces, Events, URF's and Dynamic Mesh

E.1 Mesh Interfaces

Table E.1: Mesh interfaces

Mesh Interfaces		
Mesh Interface	**Interface Zone 1**	**Interface Zone 2**
intf-ch-cyl	intf-chamber	intf-cylinder
intf-exvalve-ib	intf-exvalve-ib-fluid-ib	intf-exvalve-ib-fluid-ob-port intf-exvalve-ib-fluid-ob-vlayer
intf-exvalve-ob	intf-exvalve-ob-fluid-ch	intf-exvalve ob-fluid-vlayer
intf-int-exvalve-ib	intf-int-exvalve-ib-fluid-ib	intf-int-exvalve-ib-fluid-port
intf-int-exvalve-ob	intf-int-exvalve-ob-fluid-port	intf-int-exvalve-ob-fluid-vlayer
intf-int-invalve-ib	intf-int-invalve-ib-fluid-ib	intf-int-invalve-ib-fluid-port
intf-int-invalve-ob	intf-int-invalve-ob-fluid-port	intf-int-invalve-ob-fluid-vlayer
intf-invalve-ib	intf-invalve-ib-fluid-ib	intf-invalve-ib-fluid-ob-port intf-invalve-ib-fluid-ob-vlayer
intf-invalve-ob	intf-invalve-ob-fluid-ch	intf-invalve ob-fluid-vlayer

E.2 Events

Table E.2: Events defined for the dynamic mesh

Events	
deactivate-exvalve-zone[1]	0º
deactivate-invalve-zone[2]	0º
reduce-urf-due-to-exvalve-opening[3]	129º
activate-exvalve-zone[4]	130º
reduce-time-step-due-to-exvalve-opening[5]	130º
increase-urf-due-to-exvalve-opening[6]	135º
increase-time-step-due-to-exvalve-opening[7]	135º
reduce-urf-due-to-invalve-opening	341º
activate-invalve-zone	342º
reduce-time-step-due-to-invalve-opening	342º
increase-urf-due-to-invalve-opening	347º
increase-time-step-due-to-invalve-opening	347º
deactivate-exvalve-zone	375º
deactivate-invalve-zone	591º

E.3 URF

Table E.3: URF values when reduced

URF	
Pressure	0.2
Density	0.5
Body Forces	0.5
Momentum	0.4
Turbulent Kinetic Energy	0.1
Turbulent Dissipation rate	0.1
Turbulent Viscosity	0.5
Energy	0.5

[1]All exhaust related domains are deactivated in order to decrease calculation time.
[2]All intake related domains are deactivated in order to decrease calculation time.
[3]URF values are decreased due to sudden variations caused by valve opening.
[4]Due to valve opening, the respective zone is activated.
[5]Time-step is decreased due to sudden variations caused by valve opening. New time-step is 0.125º.
[6]URF values are increased to their previous values.
[7]Time-step is defined to its previous value - 0.25º.

E.4 Dynamic Zones

Table E.4: Dynamic mesh: Stationary zones

Stationary Zones	
Dynamic Mesh Zone	**Meshing Options**
	Cell Height
exvalve-seat	0.5 mm
intf-int-exvalve-ib-fluid-ib	0.5 mm
intf-int-exvalve-ob-fluid-vlayer	0.5 mm
invalve-seat	0.5 mm
intf-int-invalve-ib-fluid-ib	0.5 mm
intf-int-invalve-ob-fluid-vlayer	0.5 mm

Table E.5: Dynamic mesh: Rigid bodies

Rigid Bodies			
Dynamic Mesh Zone	**Motion Attributes**		**Meshing Options**
	Motion Profile	**Valve/Piston Axis** [1]	**Cell Height**
exvalve-ch	exvalve	$Y = -1$	0 mm
exvalve-ib	exvalve	$Y = -1$	0.5 mm
exvalve-ob	exvalve	$Y = -1$	0.5 mm
fluid-exvalve-ib	exvalve	$Y = -1$	---------
fluid-exvalve-vlayer	exvalve	$Y = -1$	---------
fluid-invalve-ib	invalve	$Y = 1$	---------
fluid-invalve-vlayer	invalve	$Y = 1$	---------
invalve-ch	invalve	$Y = 1$	0 mm
invalve-ib	invalve	$Y = 1$	0.5 mm
invalve-ob	invalve	$Y = 1$	0.5 mm
lower-piston	**piston-full**	$Y = 1$	2 mm
upper-piston	**piston-full**	$Y = -1$	2 mm

Table E.6: Dynamic mesh: Deforming zones

Deforming Zones					
Dynamic Mesh Zone	**Geometry Definition**			**Meshing Options**[2]	
	Cylinder Radius	**Cylinder Origin**	**Cylinder Axis**	**Zone Parameters**	
intf-exvalve-ob-fluid-ch	32 mm	$Z = -100$ mm	$Y = 1$	Min. Length Scale	0.25 mm
				Max. Length Scale	0.35 mm
				Max. Skewness	0.6 mm
intf-invalve-ob-fluid-ch	34.5 mm	$Z = -100$ mm	$Y = 1$	Min. Length Scale	0.3 mm
				Max. Length Scale	0.45 mm
				Max. Skewness	0.6 mm

[1] The direction of the axis may vary from case to case.

[2] Both *Smoothing* and *Remeshing* are activated for all deforming zones, being their methods *Spring* and *Region*, respectively.

Appendix F

Valve Motion

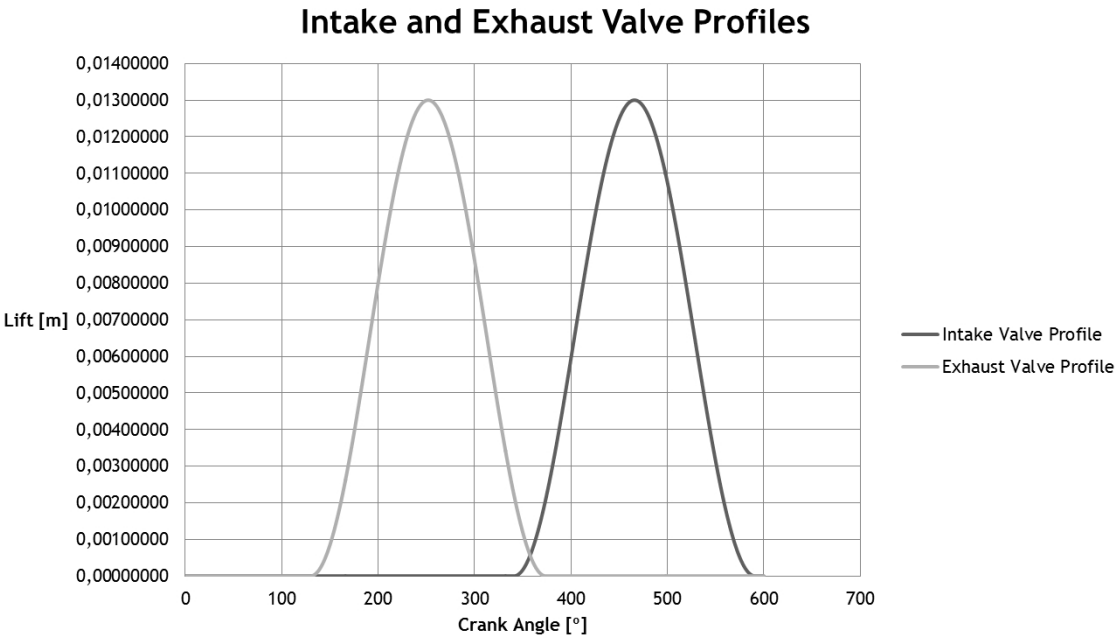

Figure F.1: Valve profiles

The exhaust valve has a maximum lift of 0.013 m and begins to open at 130º and closes at 375º of the crankshaft angle. The admission valve has a maximum lift of 0.013 m as well, and begins to open at 342º and closes at 591º of the crankshaft angle. Both profiles are sinusoidal and are defined by Eq F.1 and F.2, respectively.

$$L_{ex} = \frac{0.013}{2} \times \left(sin\left(\frac{2 \times 360}{488} \times X_{ex} + \frac{3\pi}{2} \right) + 1 \right) \tag{F.1}$$

$$L_{in} = \frac{0.013}{2} \times \left(sin\left(\frac{2 \times 360}{500} \times X_{in} + \frac{3\pi}{2} \right) + 1 \right) \tag{F.2}$$

The valve profile file is done with the following example method by using NotePad or other text editing tool. The name of choice for the valve profile is placed in "valvename" and the number of points existent for each valve is replaced where the number "5" is shown. The word "angle" is not to be altered as well as the word "lift" and all values placed after these words are the respective lift for each angle, e.g., at 0º the lift is 0.0001 m.

```
((valvename point 5 1)
(angle
0
0.25
0.5
0.75
1)
(lift
0.0001
0.00015
0.0002
0.00025
0.0003))
```

Appendix G

Article: 3D CFD Simulation of a Cold Flow Four-Stroke Opposed Piston Engine

3D CFD Simulation of a Cold Flow Four-Stroke Opposed Piston Engine

Robert Gonçalves[a], Francisco Brójo[b]

Universidade da Beira Interior, Calçada Fonte do Lameiro, 6201-001 Covilhã

[a]*Master Degree Student, Aerospace Science Department of Universidade da Beira Interior*
[b]*Assistant Professor, Aerospace Science Department of Universidade da Beira Interior*

Abstract

A CFD simulation of a four-stroke opposed piston engine has been performed. It is intended to evaluate the overall behavior and properties of in-cylinder flow, in a way that its use commercially can be achieved. Due to the inherent characteristics of an opposed piston engine, it is necessary to dimension the model, using as reference the Jumo 205E engine: both valves, as well as the combustion chamber and both exhaust and admission ports. A combustion chamber adjacent to the cylinder zone is placed in order to fit both valves. The commercial software *Fluent 14.0* is used to perform the numerical calculations. Due to the complexity inherent of this study, mostly because of the existence of moving parts, the use o dynamic meshing is necessary. The viscous model is Standard $\kappa - \epsilon$; the port entry and exit are defined as *pressure-inlet* and *pressure-outlet*, respectively. PISO and PRESTO! are the chosen methods for pressure-velocity coupling and pressure space discretization, respectively. The final results obtained were far from the expected, mainly due to the inadequate behavior of and properties of the fluid within the cylinder and ports.

Keywords: Admission, Exhaust, CFD, *Fluent*, Opposed piston, Internal combustion engine

1. Introduction

The Opposed Piston (OP) engine was initially designed in the late 1800's in Germany as an alternative to the existing engines of the time, such as the Otto engine, and was well known for its versatility and simplicity in numerous applications which included aircraft, ships, tanks, locomotives, automobiles and stationary [1]. Even though the OP concept could be applied to both two and four-stoke diesel engines, the two-stroke cycle was predominant, most likely for due to simplicity reasons.

The advantages presented by the two-stroke OP engine were so great, that several records, which were established at the time, are yet to be equaled. These records have set the regular standards which are still used today for numerous parameters in Internal Combustion (IC) engines. However, with the implementation of emission regulations in the mid-20th century, the rise of the OP engine came to a halt, mainly due to oil consumption and high emission problems, allowing the conventional four-stroke engine to develop further. Among the typical challenges which two-stroke engines faced, the main issues involved lubrication of the small-end bushes and piston-pin bosses, port traversing by the rings, side injection and torsion vibration. In four-stroke OP cycle engines, the most difficult challenge, in addition to the problems presented by the two-stroke cycle engine, was still the location of the admission and exhaust valves.

Even though the OP engine is still used in many unconstrained emission level applications, with the increasingly tighter emission regulations, the technology available today, along with the different manufacture processes and larger number of solution possibilities, many of the problems regarding the OP engine could be overcome and a wider field of application may appear.

With this in mind, the present work focuses on the construction of a four-stroke OP engine model, based on the Jumo 205E engine, followed by the numerical analysis using Computational Fluid Dynamics (CFD) tools, with the objective of verifying its reliability based on the selected valve positioning and engine geometry. Port flow behavior is also studied.

2. Planning

2.1. Geometry

The engine used as reference for this study is the two-stroke OP engine, Jumo 205E, which is then trans-

formed in order to work in a four-stroke cycle. This leads to some issues, mainly the positioning of both admission and exhaust valves. The solution proposed for this problem is a *flathead* configuration, in which two cylinder blocks would be connected, forming the combustion chamber and the necessary extra space to place the valves.

The *flathead* engine, despite its fame during the 1950's, presented a few disadvantages regarding poor in-cylinder air flow and combustion issues due to the little direct contact of the piston with the combustion chamber. Nevertheless, the *flathead* engine is still one of great interest and several ideas have been presented in order to make it more competitive with the overhead valve engine [2].

Both valves are dimensioned as well as the combustion chamber, which needs to comply with the predefined compression ratio ($c_r = 10$). The compression ratio is not equal to the engine of reference for two reasons: firstly, the model is adapted to function as a Spark Ignition (SI) engine, and secondly, the original value ($c_r = 17$) would lead to a very tight clearance volume, not allowing for the valves to move. The final geometry is built in *CATIA* and is presented in Fig. 1. The full geometry is considered due to dynamic mesh issues near the valve head during simulations; it was advised, after consulting the *ANSYS*Support Team, to use the whole domain and not half.

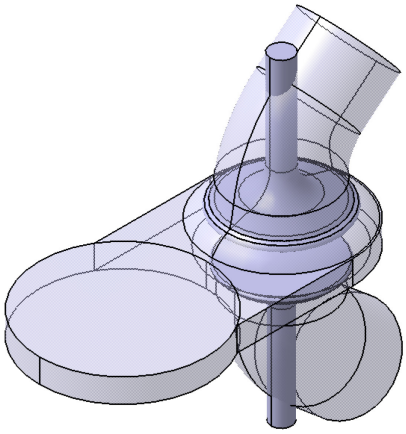

Figure 1: Domain of the model engine and valve bodies

The combustion chamber at Top Dead Center (TDC) has a clearance height of 15 *mm* and the adjacent chamber, in which the valves are located, has an "air cushion" at both valve heads. The purpose of this configuration is an attempt to have an uniform pressure around the valve head in order for the flow to enter the cylinder from all sides of the valve. The admission and exhaust valve have a head diameter of 65 *mm* and 59 *mm*, respectively. Hence that a gap with 0.2 *mm* is placed between the valve head and valve seat (see Fig. 2). Since the valves move, cells must be created and removed; however, cells cannot be created from nothing nor can be collapsed to nothing. Therefore, a layer of cells is placed in this gap in order to enable this feature. All the remaining parameters, such as bore and stroke, are the same as the original engine: 105 *mm* and 160 *mm* $\times$ 2, respectively.

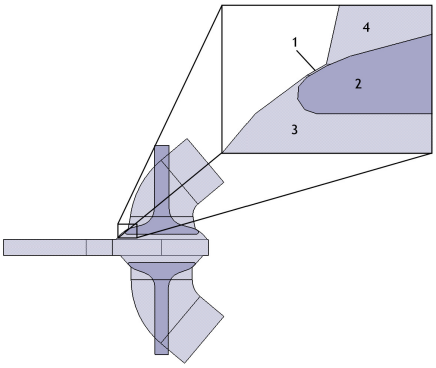

Figure 2: Detailed view of the valve gap: 1 - Gap; 2 - Valve head; 3 - Combustion chamber; 4 - Port

Afterwards, the model is decomposed into other domains. When using the *ANSYS Internal Combustion Engine Workbench*, the decomposition is done automatically for conventional overhead valve engines, however for different configurations it may be more complicated, as is the case, and requires to be done manually.*ANSYS* recommendations are to create two domains for each valve: the *inboard* and the *vlayer* [3]. The first revolves around the stem and the upper face of the valve head, while the second is the thin layer inserted in the gap previously mentioned (see Fig. 3). Both have the purpose of avoiding mesh deformation and enabling cell layering instead of remeshing these zones.

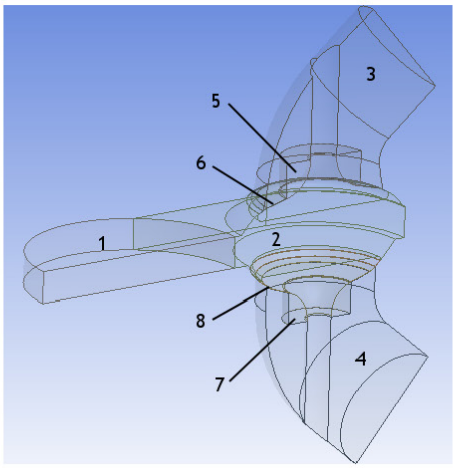

Figure 3: Symmetrical view of the decomposed geometry: 1 - cylinder; 2 - chamber; 3 - invalve-port; 4 - exvalve-port; 5 - invalve-inboard; 6 - invalve-vlayer; 7 - exvalve-inboard; 8 - exvalve-vlayer

2.2. Mesh

The quality of the mesh is directly related to the quality of the results. A structured mesh reduces computational cost, whereas an unstructured mesh is more adaptable for complex geometries. The cylinder, both *inboards* and both *vlayer* zones have a structured mesh, due to the linear movement of the pistons and valves, which enables the *layering* method. On the other hand the chamber and both ports have an unstructured mesh. The resultant mesh has a total of 3638149 cells and 933294 nodes. Hence that this number will increase due to both valve and piston movements.

The quality aspect of the mesh must be always analyzed and improved when possible. *ANSYS* suggests a possible spectrum to evaluate rather the mesh is acceptable or not in [4].

2.3. Setup

Following the geometry decomposition and meshing processes is the case setup. The commercial software *Fluent* is used to perform the calculations. Due to the nature of the case, the time solver is changed to transient and double precision is enabled.

The Energy model is activated in order to study both energy and heat transfer; the Viscous model is enabled with the Standard $\kappa - \epsilon$ model and the Standard Wall Treatment. Air is the domain fluid, with the ideal-gas-law and the piecewise-polynomial enabled for density and heat constant, respectively. Hence that the operating pressure should be defined as atmospheric (101325 *Pa*).

Four types of boundary conditions are used in this model: *wall*, *interface*, *pressure-inlet* and *pressure-outlet*. The *wall* condition is applied to all cylinder and chamber walls, as well as the piston faces, valves and port walls. All cylinder walls, as well as valve and port wall have a constant temperature of 373.15 *K*. The *interface* boundaries are applied to those where two faces of different zones are in contact. The *pressure-inlet* is applied to the intake and *pressure-outlet* to the exhaust faces. *Pressure-inlet* is adequate when the intake pressure is known, but flow rate and/or velocity is not. Also, it is suitable for both compressible and incompressible flows. The *pressure-outlet* normally presents better rate of convergence results when *backflow* occurs than the *outflow* boundary condition.

As both pistons and both valves move, the mesh surrounding these parts start to deform. In order to avoid this deformation, dynamic meshing is employed: *layering*, *remeshing* and *Smoothing*. *In-cylinder* is also activated, where parameters such as engine speed, crank angle step size and crank period are defined (see Table 1). *Events* are created to change any parameter during the simulation, such as activating or deactivating cell zones, changing time-steps or Under-Relaxation Factors (URF's) and creating or deleting sliding interfaces.

Table 1: *In-cylinder* parameters

Parameters	
Crankshaft Speed	2500 *rpm*
Starting Crank Angle	0
Crank Period	600
Crank Angle Step Size	0.25
Crank Radius	80 *mm*
Connecting Rod Length	290 *mm*
Piston Pin Offset	0 *mm*
Piston Stroke Cutoff	0 *mm*
Minimum Valve Lift	0 *mm*

The *dynamic mesh zones* are defined as *stationary*, *rigid body* or *deforming*. *Stationary zones*, as the word suggests, are the boundaries or zones that do not move. Normally, these are only defined when the adjacent zones are moving. *Rigid bodies* are those that have a rigid body behavior, without deforming its mesh. The *deforming zones* define the zones that are subjected to mesh deformations.

In the solution method, PISO is chosen for the

pressure-velocity coupling scheme; PRESTO!is enabled for the pressure discretization method; the Green-Gauss Node-Based scheme is chosen for the gradient spatial discretization; Second-order Upwind scheme is used for all variables with the exception of dissipation rate (ϵ). Finally, the initial values for URF's are defined (see Table 2).

Table 2: Under-Relaxation Factors

URF	
Pressure	0.3
Density	1
Body Forces	1
Momentum	0.7
Turbulent Kinetic Energy	0.4
Turbulent Dissipation Rate	0.4
Turbulent Viscosity	1
Energy	1

The solution is initialized with appropriate values: 323.15 K for temperature (cylinder and chamber zones are patched with 1081 K) and pressure is assigned with 0 Pa (cylinder and chamber, as well, are patched with 3000000 Pa). Finally, the solution calculation begins with 2440 time steps, 40 iterations per time step.

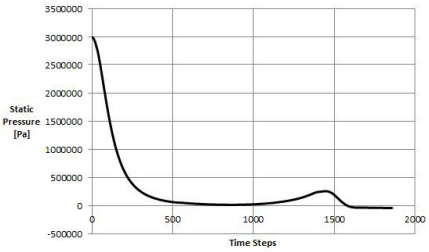

Figure 4: In-cylinder static pressure

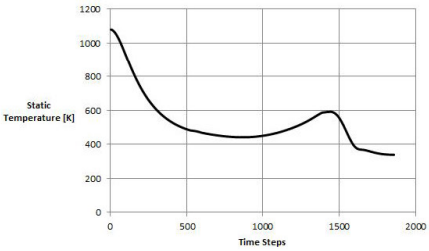

Figure 5: In-cylinder static temperature

3. Results

Over the course of one year, numerous simulations were performed, in which the majority was not concluded due to various obstacles and problems: geometry and computational cost were the main issues faced. Due to the second issue, the present simulation did not conclude all 2440 time steps; however, among all the simulations performed, the present one displayed better results.

As expected, during the expansion stage (the initial 520 time steps) a decrease of both pressure and temperature is visible within the cylinder as presented in Fig. 4 and Fig. 5, respectively.

During the exhaust process, the velocity in the gap near the valve head increases rapidly due to the very tight opening (Fig. 6) and then slowly decreases until 190. After this point, the flow separates at the rear end of the valve (Fig. 7) and the Mach number gradually begins to increase, reaching a maximum of Mach 2.2 at TDC position. It is believed that these abnormal values appear mainly due to the geometry of the cylinder/chamber; as both pistons move towards the TDC, fluid is pushed through the narrow opening into the chamber and flows directly through the front and lateral sides of the valve gap, meaning that nearly half the valve is not used properly.

Slightly after the admission valve opens, both pressure and temperature decrease again, since in-cylinder pressure is greater than the admission port and so the flow exits the cylinder through the admission valve. It is known that this occurrence is usual, however it is not desirable, especially when it occurs for long periods of time. Only when the in-cylinder pressure decreases to values near or lower than the admission port does the flow enter the cylinder (see Fig. 8). Similarly to what happens at the exhaust valve, only one side of the admission valve functions properly; due to the suction created the fluid also enters the cylinder directly from one side of the valve leading to a poor performance of the other remaining half. Fig. 9 shows precisely that near the valve throat. Also visible in Fig. 9, is the high value of Mach number, not at the valve throat, but at the passage from the chamber to the cylinder.

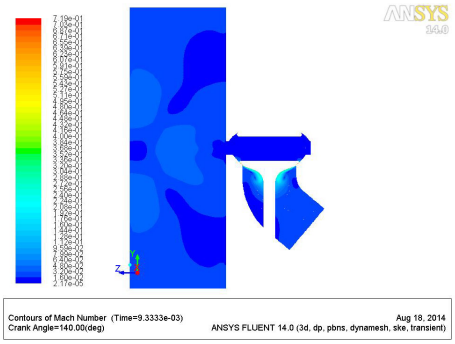

Figure 6: Contours of Mach number at 140crank angle

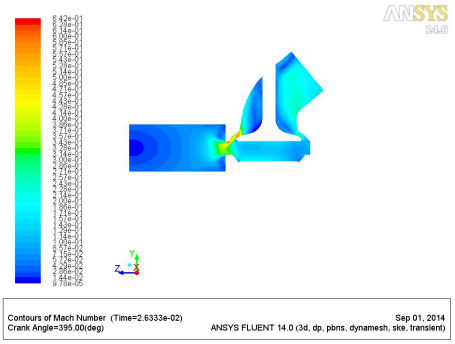

Figure 8: Contours of Mach number at 395crank angle

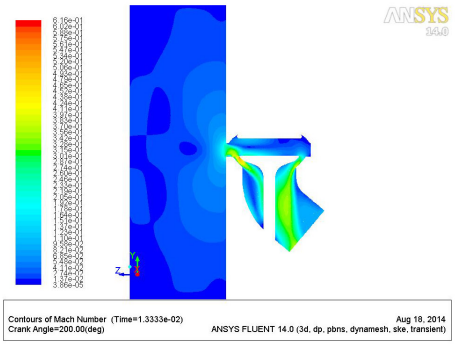

Figure 7: Contours of Mach number at 200 crank angle

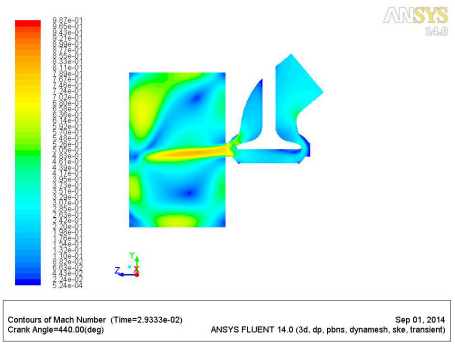

Figure 9: Contours of Mach number at 440 crank angle

4. Discussion

As for the results obtained from the CFD analysis, these can be brought down to three stages: expansion, exhaust and admission stages. The expansion stage performed as expected, with both pressure and temperature decreasing. When the exhaust valve opens, initially, fluid is pushed out through the whole surrounding of the valve; however, as this stage continues, Mach number at the valve throat reaches unbearable values, as well as the in-cylinder pressure and temperature increase due to the inability of the valve to expel the gases. Finally, the admission stage, similarly to the previous one, performs well at the beginning, but the duration of reverse flow from the cylinder to the admission port is far too long. Plus, the valve cannot deliver the amount of air necessary at the needed rate and, at the passage from chamber to cylinder, velocity reaches once again very high values.

It is the authors opinion that adapting an OP engine to function at a four-stroke cycle still cannot be dismissed, however the engine of reference for this case is to large in order to function as so, since neither the exhaust and admission processes produced the expected results. Possibly, OP engines with a smaller bore and/or stroke can be used to be adapted as a four-stroke.

[1] D. Johnson, M. Wahl, F. Redon, E. Dion, S. McIntyre, G. Regner, R. Herold, Opposed-piston two-stroke diesel engine-a renaissance, in: Symposium on International Automotive Technology (SIAT), 2011.
[2] M. Clements, Cylinder head and valve configuration, uS Patent 6,328,012 (Dec. 11 2001).
[3] ANSYS, Ic engine system, in: Automotive Simulation World Congress, 2012.
[4] Introduction to ansys - meshing (2012).